Pergamon

Journal of Structural Geology, Vol. 19, Nos 3–4, pp. 413 to 441, 1997

0191-8141/97 $17.00 + 0.00

PII: S0191-8141(96)00116-2

# Progressive evolution of a fault-related fold pair from growth strata geometries, Sant Llorenç de Morunys, SE Pyrenees

MARY FORD, EDWARD A. WILLIAMS and ANDREA ARTONI

Geologisches Institut, ETH-Zentrum, 8092 Zürich, Switzerland

JAUME VERGÉS

Grup de Geodinàmica i Anàlisi de Conques, Departament de Geologia Dinàmica, Geofísica i Paleontologia, Universitat de Barcelona, Mart i Franquès s/n, 08071 Barcelona, Spain

and

STUART HARDY

Institute of Earth Sciences (Jaume Almera), Consejo Superior de Investigaciones Cientificas, c/Lluis Sole i Sabaris s/n, 08028 Barcelona, Spain

(*Received* 26 *February* 1996; *accepted in revised form* 21 *October* 1996)

**Abstract**—New structural–stratigraphical mapping constrains the three-dimensional kinematics and mechanisms of Eocene–Oligocene growth folding at Sant Llorenç de Morunys (NE Ebro basin, Spain). A 1 km wide sub-vertical panel of syntectonic alluvial gravels passes southwards via a highly asymmetrical growth fold-pair to shallowly-dipping strata. The axial surface of the anticline comprises either continuous or en échelon segments while that of the syncline is concave and usually continuous. While converging upwards, the axial surfaces do not define growth triangles. Principal and subsidiary growth unconformities and thickness changes occur across both axial surfaces and the common limb. Dips within the common limb decrease up-stratigraphy and up-dip. Mesostructures indicate that internal deformation was ongoing during folding at all stratigraphical levels, and concentration of cleavage in the syncline indicates that this hinge was essentially fixed. Sequential restoration of three profiles shows that folds amplified principally by limb rotation but incorporated minor passive hinge migration. Particle movement vectors, generated by section restoration, are arcuate about a hinterland pinpoint. A new trishear model of fault propagation folding involving non-rigid limb rotation reproduces the rounded hinge forms, thickening geometries and limb dip variations observed. Simple kink band migration models (fixed axis and constant thickness theories) do not replicate these features. 

## INTRODUCTION

This paper investigates two outstanding problems in the realm of fault-related folding at high levels in the crust: (1) the evolutionary nature of fold amplification and (2) the deformational mechanisms involved. Understanding the first of these is facilitated in cases where sedimentation was coeval with both subsidence and contractional deformation, leading to the preservation of growth strata which record the development of associated fold structures. Discussion has focused on two principal mechanisms by which folds can amplify, these being limb lengthening and limb rotation (Fig. 1). Well known categories of fault-related folds which may show these mechanisms are fault-bend (Rich, 1934), fault-propagation (Elliott, 1976; Williams and Chapman, 1983; Mitra, 1990; Suppe and Medwedeff, 1990) and detachment folds (Jamison, 1987; Poblet and Hardy, 1995; Epard and Groshong, 1995).

Geometrical–numerical models of fault-bend and fault-propagation folds have been developed in which limb lengthening due to kink band migration (Fig. 1a) is the sole formative mechanism (Suppe, 1983; Suppe and Medwedeff, 1990). Other, similar, models of detachment folds with growth strata (Hardy and Poblet, 1994) and fault-propagation folds (Erslev, 1991) involve limb rotation (Fig. 1b). In the kink-band migration model of fault-propagation folds (Suppe *et al.*, 1992) growth strata within growth triangles of the steep forelimb show no variation in dip or thickness up-section (Fig. 1a). Once transferred into the steep limb through a growth axial surface (Fig. 1a), strata do not undergo further strain, and interlimb angle and axial plane dip remain constant through the growth strata. In contrast, a limb rotation model (Hardy and Poblet, 1994), for similar sediment accumulation and deformation rates, shows clear changes of growth stratal dip and thickness, both up-dip and up-section on the steep forelimb (Fig. 1b).

Syntectonic deposits of the immediate footwall of orogenic fronts frequently preserve growth geometries that can determine both the age of motion of the structures as well as their kinematics (DeCelles *et al.*, 1991a; Burbank and Vergés, 1994). These semi-consolidated sediments are typically subject to contractional faulting and folding at the topographic surface and at shallow depths under non- to very low grade meta-

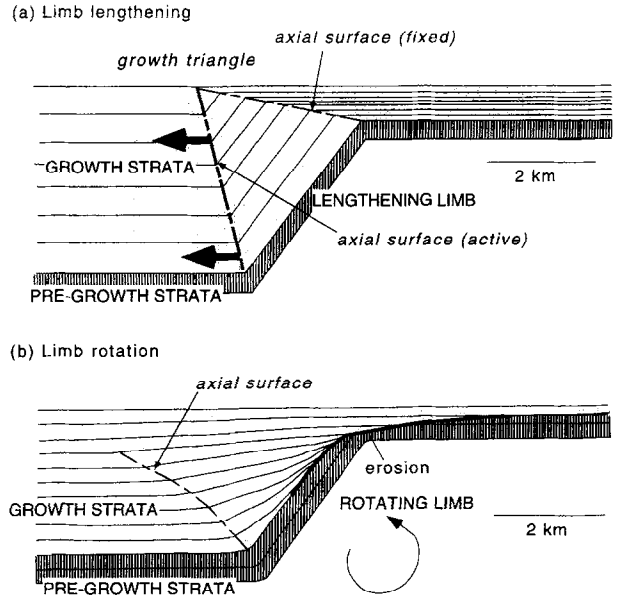


Fig. 1. Models incorporating the two principal processes (limb lengthening and limb rotation) which can generate a growth fold pair in the upper crust. The two models show distinctive growth stratal geometries. (a) Limb lengthening is illustrated here by the fixed-axis kink band migration model of Suppe and Medwedeff (1990). (b) The limb rotation model of Hardy and Poblet (1995) exhibits progressive stratal rotation and thinning.

morphic conditions. We focus on such a setting at Sant Llorenç de Morunys, located at the north-east margin of the Ebro basin, Spain (Fig. 2), where fold structures amplified synchronously with accumulation of late Eocene–Oligocene gravelly alluvium shed from the south-east Pyrenees. These folds are now spectacularly exposed due to deep incision by modern rivers.

In earlier descriptions of the structural geometries of this area Riba (1973, 1976a,b) defined the terms *progressive unconformity* and *cumulative wedge*, as well as interpreting 'syntectonic' and 'pre-orogenic' sequences, i.e. growth and pre-growth strata of subsequent terminology. He suggested that a single progressive unconformity is a syntectonic cumulative wedge system attached to a tilting depositional surface, in turn linked to an uplifting structure (typically asymmetrical, antiformal buckle folds or steep contraction faults). The progressive development of a cumulative wedge depends on the relative rates of uplift, rotation and sedimentation and can result in rotative onlap or rotative offlap geometries. Riba and subsequent workers (Anadón *et al.*, 1986) in the Ebro basin region thus envisaged rotation as the primary structural process related to wedge growth. However, the genetic model proposed for the geometries at Sant Llorenç de Morunys (Riba, 1976b, fig. 8) does not relate rotation specifically to fold development, and does not reproduce the gross upward convergence of the synclinal and anticlinal axial surfaces observed.

Our aim in this paper is to determine which mechanisms were of primary importance in the development of this complex growth fold structure by a study of its three-dimensional evolution. In order to achieve this, detailed structural and stratigraphical field data have been converted into three serial cross-sections of exposed growth geometries which are restored in a series of time-related steps. We use these data to discuss the evolution of larger scale fold and thrust geometries. Allied to this, numerical forward models of contrasting folding mechanisms have been adapted (from Suppe and Medwedeff, 1990) and developed in order to reproduce and compare with the evolutionary-geometrical features observed in the field and in our restorations.

Two main conclusions are drawn: (1) the fold pair grew primarily by limb rotation with minor passive hinge migration caused by the wedge-like forms of the accumulating sedimentary bodies, and (2) a modified trishear model is quite successful in replicating the rounded hinge forms, stratal geometries and limb dip variations developed in the Sant Llorenç de Morunys growth structure, while the widely applied kink band migration fold models do not replicate the observed geometries.

## GEOLOGICAL SETTING

The Sant Llorenç de Morunys area is located 1–2 km south of the present day mountain front of the south-eastern Pyrenees (Fig. 2a). The folded clastic marine and continental succession here contains stratal geometries and internal (intraformational) unconformities studied by a number of researchers since the 1930s, whose work is fully summarized by Riba (1967, 1973, 1976a,b). The structure at Sant Llorenç de Morunys is one of a series located basinward of the south Pyrenean thrust front (Nichols, 1987; Burbank and Vergés, 1994) which deformed sediments accumulating in the proximal part of the Ebro foreland basin. This basin subsided in response to the emplacement of a stack of thrust sheets during south-directed shortening from the latest Cretaceous to the Oligocene in the east, to the early Miocene in the west (Fig. 2; Burbank *et al.*, 1992; Puigdefàbregas *et al.*, 1992; Vergés, 1993). The basin fill records early to mid Eocene marine conditions followed by late Eocene–Oligocene continental conditions (Puigdefàbregas and Soquet, 1986).

The Sant Llorenç de Morunys growth structure (Riba, 1973, 1976a,b) lies in the footwall of the frontal 7° north-dipping Vallfogona thrust (Figs 2b & 3). This fault places mainly Eocene carbonates and marls of the Port del Compte and Cadí thrust sheets, respectively (Fig. 2b) over a marine mixed clastic–carbonate succession (the Banyoles and Igualada marls) and an overlying conglomerate-rich succession cropping out over a large area of the north-eastern Ebro basin (the Berga Conglomerate Formation of Riba, 1976b and Mató *et al.*, 1994). The > 2.4 km thick conglomerate succession is interpreted to be late Eocene–Oligocene in age by comparison with the equivalent succession at Oliana (Fig. 2b; Burbank *et al.*,

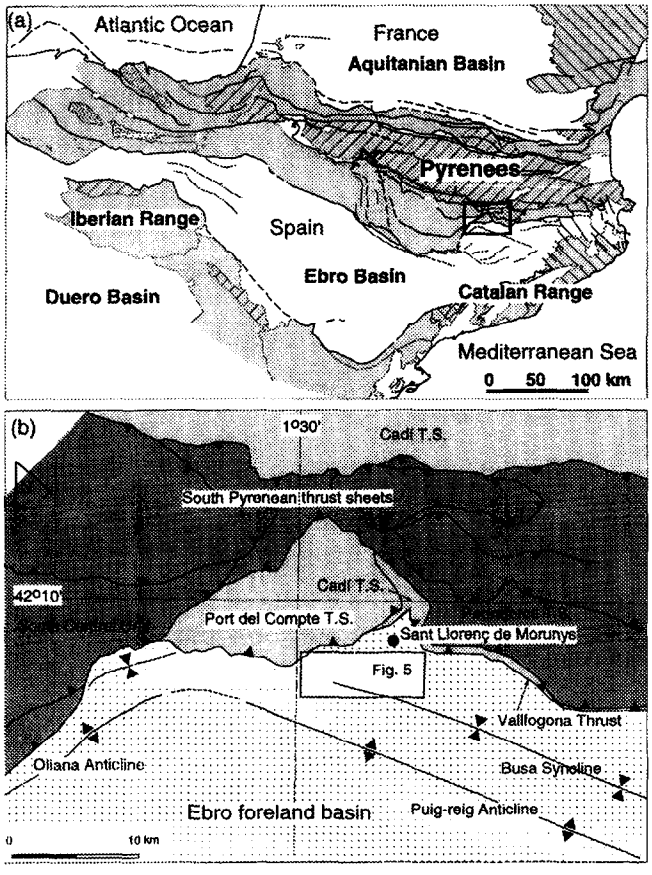


Fig. 2. (a) Regional map of the Pyrenees showing the location of the study area. (b) Structural map showing the South Pyrenean zone thrust sheets and their relationships to the north-east Ebro basin sediments around the Sant Llorenç de Morunys growth structure.

1992; Vergés *et al.*, 1996) and its rapid conformable facies transition (over ca 10 m) from the biostratigraphically dated mid Eocene marine succession.

The Sant Llorenç de Morunys structure can be conveniently divided into (1) an overturned to sub-vertical (3 km thick) panel comprising the Banyoles–Igualada marls and lower alluvial conglomerates, succeeded to the south by (2) a macroscopic anticline–syncline couplet, showing growth strata developed entirely in similar conglomerates (Figs 3–5). These structural divisions are separated in the west by a spectacular angular unconformity, whereas to the east there is an uninterrupted (southward) transition from overturned to shallowly-dipping strata (Fig. 5). The exposed growth fold pair and the steep panel therefore belong to a single large fold that increases in size northward in a linear manner so that, at the marine–continental transition, the common limb length is 1.4 km (Fig. 3b). North of the exposed fold pair the anticlinal closure lies above the level of erosion (Fig. 3a). As a consequence of a shallow (1°) WNW axial plunge and increasing amplitude and wavelength eastward, the principal unconformity and growth anticline are above present erosion level in the eastern sector of the study area whereas to the west they are concealed beneath younger, shallowly-dipping post-growth conglomerates. Southwards, towards the centre of the Ebro basin, coeval finer-grained continental facies are folded by the Puig-reig growth anticline (Fig. 2b; Vergés, 1993).

The steep and overturned bedding dips in the Sant Llorenç de Morunys structure suggest that an origin as a fault-bend fold is unlikely (see Suppe and Medwedeff, 1990, p. 412). The lack of features diagnostic of detachment folds (e.g. collapsed hinge antiforms), the strong asymmetry of the structure and its close association with thrusts of the same vergence make it likely that this structure developed as a fault-propagation fold pair ahead of a low-angle blind thrust (Fig. 3a). Other than the Vallfogona thrust no emergent faults are associated with the growth structure (Figs 2b & 5). This fault is interpreted as an anticlinal breakthrough thrust. As it is sealed by the uppermost beds of the Berga Conglomerates to the west of the study area the Vallfogona thrust was active during fold growth and by inference moved simultaneously with the blind thrust. The present re-entrant trace of this thrust (Fig. 2b) is an erosional geometry. Seismic data (Vergés, 1993) reveal flat-lying reflectors ca 2.2 km below the current erosion level (Fig. 3a) interpreted here as bedding. These data limit the vertical dimension of the growth fold, requiring the presence of a sub-horizontal fault between steep strata and the flat reflectors (Vergés, 1993; Fig. 3a).

## *Methods*

Apart from the maps of Riba (1973, 1976b), which were based on the combination of interpretation of vertical (1:33,000 scale) aerial photographs and field-work, no published geological map is available for this area. In June–August, 1995 structural and stratigraphical data, from an area of approximately 36 km$^2$, were surveyed on to 1:5000 digital topographical and ortho-photomaps, which have been compiled in Fig. 5. Selected critical areas were mapped at a scale of 1:1250. Attention was paid to mapping distinctive reference formations and marker horizons, to establish a detailed lithostratigraphic scheme (Fig. 4). Minor structures were routinely measured during mapping. Three vertical cross-sections (see Fig. 5 for location) were constructed normal to stereographically derived fold trends (Fig. 6) by projecting data parallel to local fold axes. Corrections were made for apparent dip. A careful check was kept on the viability of projecting stratigraphical and structural data onto section planes in order to test the cylindricity of the folds. Minor changes in fold axial plunge and the wedging geometry of growth strata in sub-vertically dipping sections indicate that the structure is cylindroidal. Projection distances, usually $<750$ m and a maximum of 2 km (WNW of profile 3), are therefore considered valid. Detailed geometries of growth strata were analysed and the profiles were retrodeformed in a series of up to eight steps in order to understand the sequence of growth. The serial profiles reveal the three-dimensional variation in growth fold history.

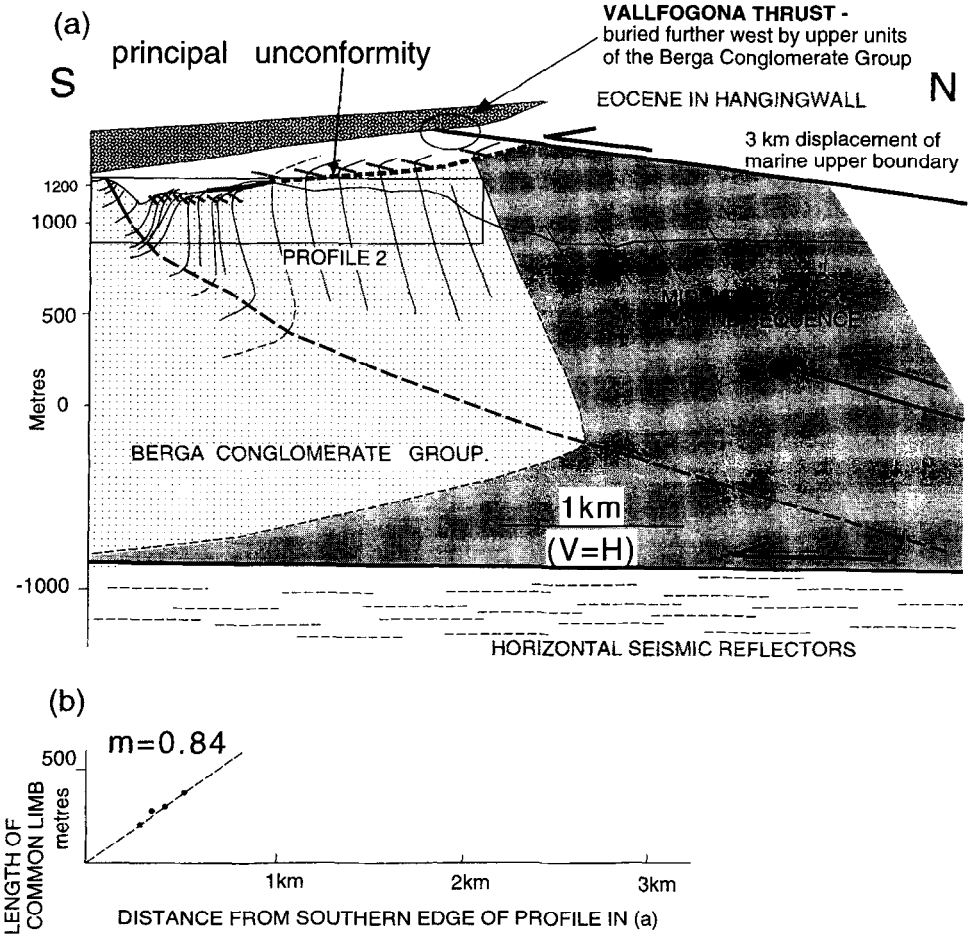


Fig. 3. (a) Simplified profile showing an interpretation of the regional context of profile 2 (Fig. 9; boxed area on this figure). The position of the blind thrust is predicted by the trishear fault-propagation fold model. Sub-horizontal seismic reflectors and flat thrust from Vergés (1993). (b) Plot of common limb length against horizontal distance for the exposed growth fold pair. Northward extrapolation predicts a common limb length of 1.4 km at the marine–continental boundary.

*Stratigraphy*

Eleven formations within the Berga Conglomerate Group at Sant Llorenç de Morunys (Fig. 4) are defined by combinations of lithological and sedimentary facies criteria, in particular (1) ratio of conglomerate to sandstone, (2) textural maturity, (3) clast petrography of conglomerates, (4) presence of distinctive facies, and (5) bed thickness. Sandstone-rich units (Fig. 4) comprise 20–30% of coarse-grained and pebbly sandstone, and rare siltstone lithologies. An earlier internal stratigraphy of the Berga Conglomerates (Riba, 1967, 1976a,b) was based on aerial photograph mapping of seven 'key (conglomerate) beds', certain of which form boundaries between four members. In some cases these 'key beds' correspond to the boundaries of mapping units defined in Fig. 4, but most are internal to newly defined units. For this reason the scheme of Riba (1976b) is not used in this paper. Most of the newly defined units (Figs 4 & 5) are represented throughout the growth fold, allowing correlation across the area. Two (upper and lower) marker horizons within the Pont de les Cases Formation (Fig. 4) also facilitate stratigraphical correlation. Variations in unit thickness and character, resulting in the termination of some formations, occur parallel to the axis of the growth structure (Fig. 4). However, the most marked thickness changes occur across strike. Units define wedge-like bodies with major thinning northward across the synclinal axial plane and particularly across the anticlinal hinge with its associated complex of unconformities.

*Sedimentology*

Characteristic lithologies include granule to small boulder conglomerates, lithic arenites and siltstones. In detail, a variety of gravel facies predominate, defined by combinations of grading type (Nemec *et al.*, 1984), clast support system, fabric and stratification. Typical facies are polymodal, massive, very poorly sorted, small pebble to large cobble conglomerates, characterized by a coarse (sand-granule to small pebble) matrix locally rich enough to support the modal clasts, which are in weak point contact. Other facies show better developed clast-supported frameworks. Massive, matrix-supported pebble–cobble conglomerates with irregularly-distribu-

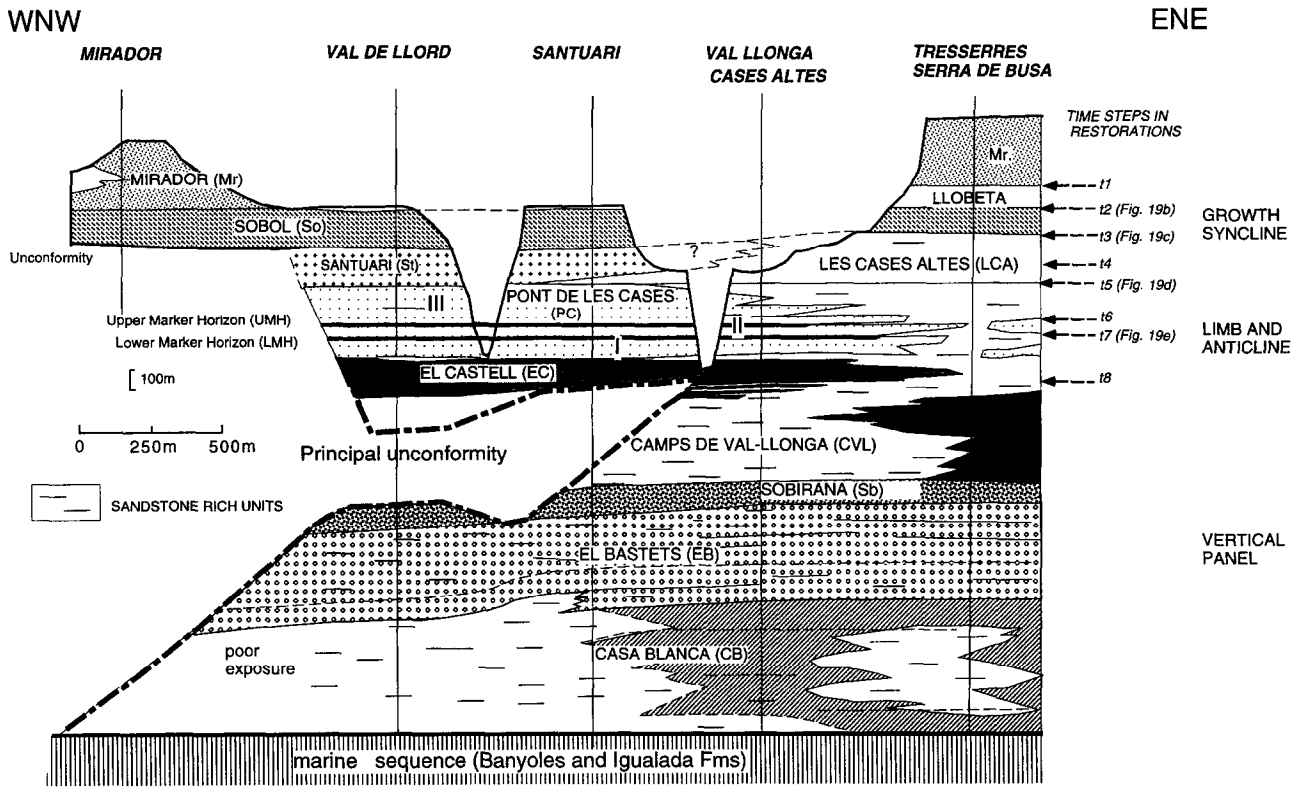


Fig. 4. WNW–ESE stratigraphical scheme erected for the Berga Conglomerate Group of Sant Llorenç de Morunys. Thicknesses above the El Castell Formation are not scaled as they vary across the growth fold at right angles to the plane of this diagram. Patterned units are conglomerate-dominated. Abbreviations of formation names used in later figures are shown in brackets. Restoration steps of Figs 19 and 20 are shown as t1 to t8.

ted and low density gravel clast content, contain a matrix of reddened (5R4/6) silty sandstone plus variable amounts of granule gravel. Clast assemblages are polymict and stratigraphically variable, being dominated by sedimentary clast types. Large framework clasts are rounded to well-rounded blades to sub-spheroids. Bed thicknesses range from 0.05 m to 5.5 m. Sandstone facies are frequently present as caps on conglomerate beds. They are typically horizontally parallel-laminated, but form a continuum to three-dimensional undulatory–sinusoidal stratification.

The predominant conglomerate facies contain many features of alluvial sub-aerial mass-flow (Nemec and Steel, 1984) and, to a lesser extent, stream-flow deposits (Allen, 1981). Rare viscous debris flow facies suggest allied settings to medial–distal slopes of steep (small radius) alluvial fans (Rust and Koster, 1984). Bed thicknesses, stratification and fabrics indicate that modal gravel emplacement occurred as $<1$ m thick event deposits. Smaller volumes of gravel were deposited grain by grain from turbulent flows. This suggests that structural growth was related to bed-scale aggradational events, and that the prominent stratal contacts visible in the field represent larger than average non-depositional periods (diastem to possibly paraconformity status). Remapping and 1:25 scale sequence logging demonstrates that the 'key beds' of Riba (1967, 1976a,b) are metre-scale sequences of individual conglomerate (and sandstone) beds *sensu stricto*, and are therefore multi-event deposits. Layering in high-relief natural exposures (bed contacts, fabric and other stratification) is generally concordant within formations and to their boundaries. Exceptions occur where specific types of growth-related unconformities are involved. Discordances due to intrinsic alluvial processes (DeCelles *et al.*, 1991b) are comparatively few. Progressive changes of individual bed thickness are visible across growth fold axial surfaces; stratification, therefore, is systematically related to fold structures.

## STRUCTURAL GEOMETRY

### *Geometry of the growth fold pair*

Poles to bedding (Fig. 6) indicate that the mean fold axis trends 1°–284°. Subdivision of the data does not reveal significant departures from this regional trend, except southeast of the Alt Cardener river (Fig. 5) where the growth syncline is best exposed and its axis plunges 5°–105° (Fig. 6d). South of the growth syncline, shallow northward dips define a distinct upright open fold, named the Busa syncline (Figs 2b & 5).

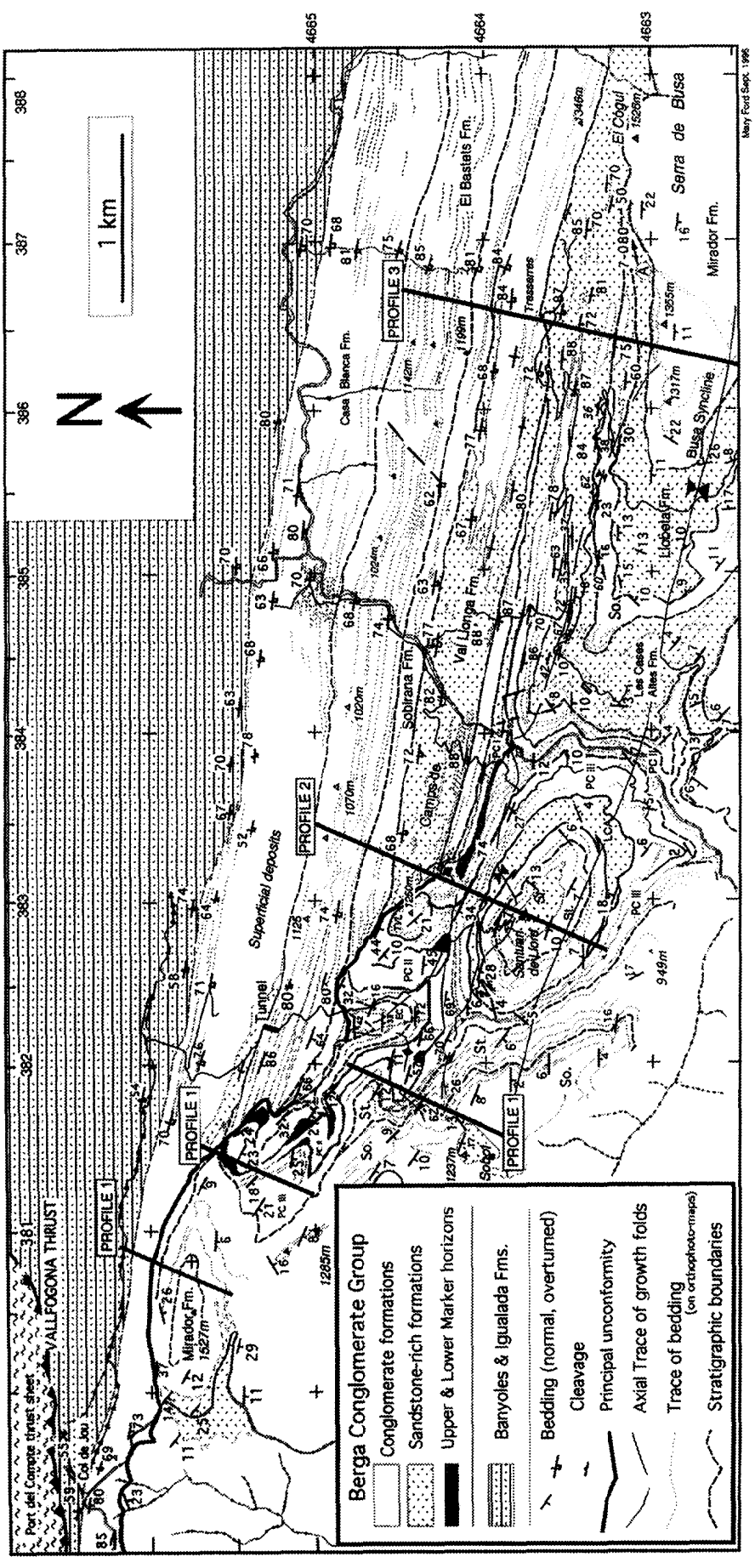


Fig. 5. Geological map of the Sant Llorenç de Morunys growth structure showing main stratigraphical units, representative bedding and cleavage readings, fold axial surface traces and profile lines. Key to abbreviations of stratigraphical units given in Fig. 4.

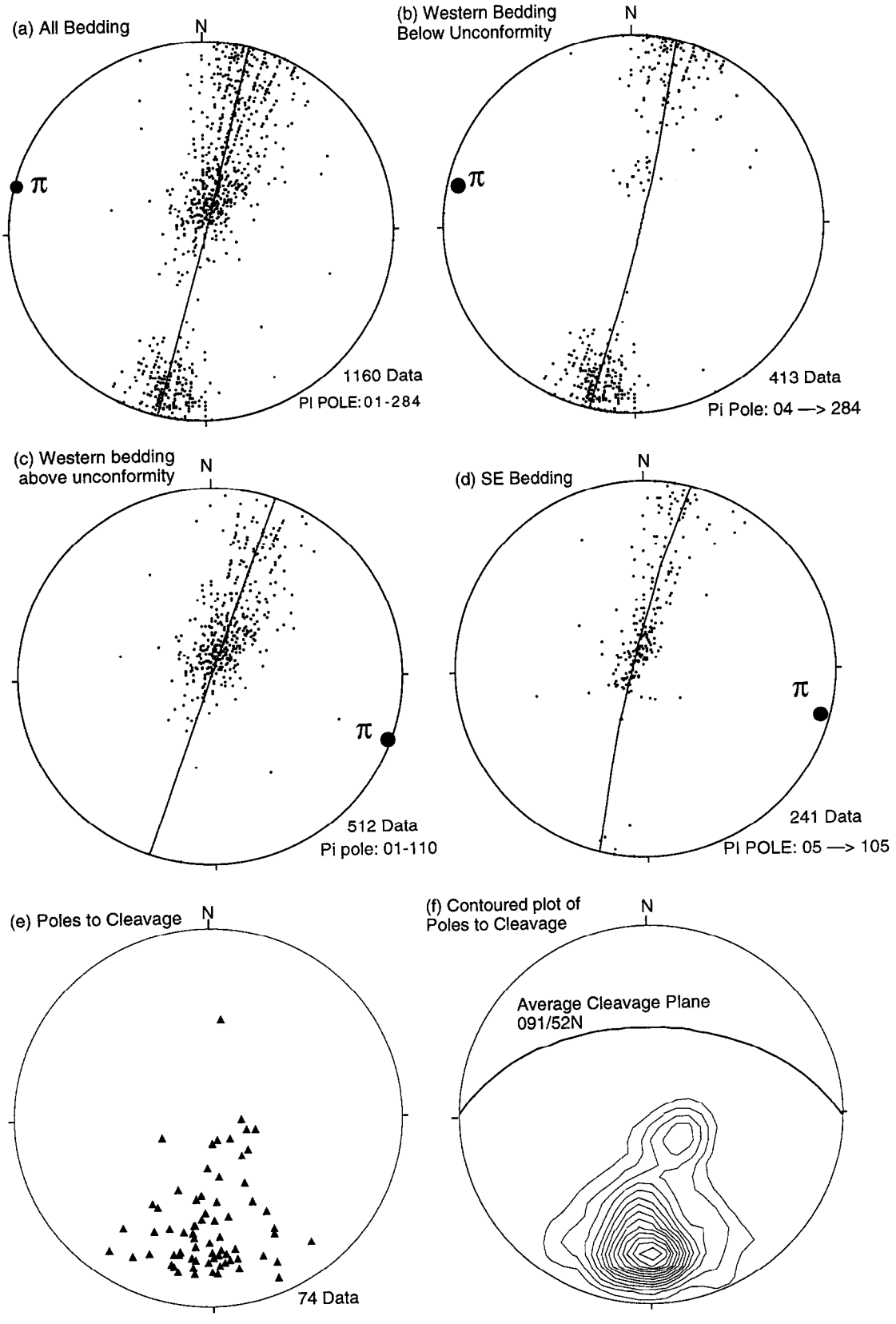


Fig. 6. Lower hemisphere, equal area stereoplots of poles to bedding (a–d) and cleavage (e). (f) shows contoured poles to cleavage. Filled circles are ($\pi$) fold axes.

Growth fold geometries vary along strike and up-section. Hinges are everywhere rounded. Fold amplitude dies out upward towards younger growth strata and the fold pair increases in size from west to east. The length of the common limb in the upper marker horizon is 250 m on profile 1 (Figs 7 & 8), 300 m on profile 2 (Figs 9 & 10) 1 km to the east and approximately 700 m on profile 3 (Figs 11 & 12), 3 km further east. The latter is a minimum estimate as the anticline has been eroded.

Hinge points are identified for various stratigraphic levels on the profiles (Figs 7b, 9b & 11b) and joined to give synclinal and anticlinal axial surfaces which converge upwards but do not meet to define a growth triangle. On profile 1, the convergence of the axial surfaces (ca 27°) decreases upward until they become parallel (Fig. 7b). The hinge points join to give continuous curved axial surfaces that steepen upward (Figs 7b & 8). However, in the Camps de Val-Llonga Formation there is a discontinuity in the axial surface of the anticline and below this unit the axial plane terminates. The anticlinal closure for the Sobirana Formation and older strata must have lain above the level of the principal unconformity. This jump in the level of the anticlinal axial surface occurs across a zone of complex dips (20° dip fan) which passes upward into the principal unconformity. The intensity of folding decreases up-section until it cannot be recognised in the upper levels of the Sobol Formation (Figs 7 & 8).

On profile 2 (Figs 9 & 10) the hinge points of the syncline join to give a continuous, curved axial surface which steepens upward over 80% of its trace, before shallowing slightly in the upper (Sobol Formation) part of the section. In contrast, the hinge points of the anticline can only be joined for short en échelon segments, stepping downwards up-section to describe a sub-horizontal array. The hinge zone of the anticline is superbly exposed on the eastern side of Tossal de Val-Llonga (Figs 10, 13 & 14). A detailed profile through this area (Figs 13 & 14), shows that the individual segments of the axial surface lie within stratigraphic packages defined by marked unconformities in the lower parts of the closure (e.g. El Castell Formation) and within overlapping and offlapping units at higher levels (Pont de les Cases Formation). A finer segmentation of the axial plane can be defined within the hinge zone but the overall en échelon pattern does not change. The dips of the axial plane segments shallow down-section. Such a discontinuity along an axial surface develops when non-parallel layers are folded. This phenomenon is well known in polydeformed terrains (Ramsay, 1967, p. 120). Offsets along the axial surface become more pronounced as the angular difference between layers increases. Thus the greatest jumps in the axial surface of the growth anticline (Figs 9 & 13) mark periods of significant erosion (or non-deposition) and tilting (folding).

On profile 3 (Figs 11 & 12) the synclinal axial surface curves upward with a major discontinuity across the zone of composite growth onlap–offlap at the top of the Pont de les Cases Formation, and can be traced into the uppermost stratigraphic levels (Mirador Formation) on the Serra de Busa (Fig. 11). The anticlinal closure, which we assume lies above the present-day level of erosion for strata below the top of the Pont de les Cases Formation, can be defined in younger strata (exposed at point A in Fig. 11a) up to the middle of the Mirador Formation (Riba, 1976b). Thus both axial surfaces on profile 3 jump abruptly closer together across the zone of composite growth offlap–onlap at the top of the Pont de les Cases Formation. Two pairs of converging axial surfaces can thus be defined, one with a wide convergence angle below this level and a second with a smaller convergence angle from this level into the Mirador Formation.

*Unconformities and depositional geometries*

The spatial arrangement of unconformities and sedimentary wedge systems records the interaction of structural and sedimentary processes across growth folds. The established terms, progressive unconformity and cumulative wedge (Riba, 1976b), are considered too general to be of use here in describing the observed geometries. Accordingly, more specific geometries are defined (Fig. 16) and a revised terminology is introduced. The simplest and best known geometries are growth onlap, growth overlap and growth offlap (Fig. 16a & b). A system of sedimentary wedges that pinch out together at the tip of an unconformity without showing any of these geometries is described here as an apical wedge (Fig. 16d). Unconformities associated with growth folds may be due either to a single period of local non-deposition or erosion associated with deformation (Fig. 16e) or to erosion that gradually migrated basinward as the fold pair developed (Fig. 16f). Along such an unconformity the time gap represented becomes greater toward the hinterland (Fig. 16f). Toward the basin the unconformity gradually, or abruptly, becomes bedding-parallel. We describe this as a growth un conformity. Growth unconformities can be either simple or composite. Composite growth unconformities show a three-dimensional arrangement of minor erosion surfaces that merge towards the hinterland and become conformities toward the basin (Fig. 16f). Local internal unconformities that become bedding parallel both toward the foreland and the hinterland can be caused by (alluvial) incision-infill (Fig. 16c) or by tilting and erosion (Fig. 16e). Within a growth syncline a particularly complex geometry can be generated by growth offlap followed by growth onlap (Fig. 16g). Any combination of the features described in Fig. 16 can produce a progressive unconformity or cumulative wedge system. Simple thinning of stratigraphical units (wedging) may also be produced by progressive decrease in bed thickness across growth axial surfaces.

A complex array of unconformities and sedimentary wedges has been mapped within the Sant Llorenç de Morunys growth strata (Figs 7–12). The growth fold pair is associated with one principal growth unconformity

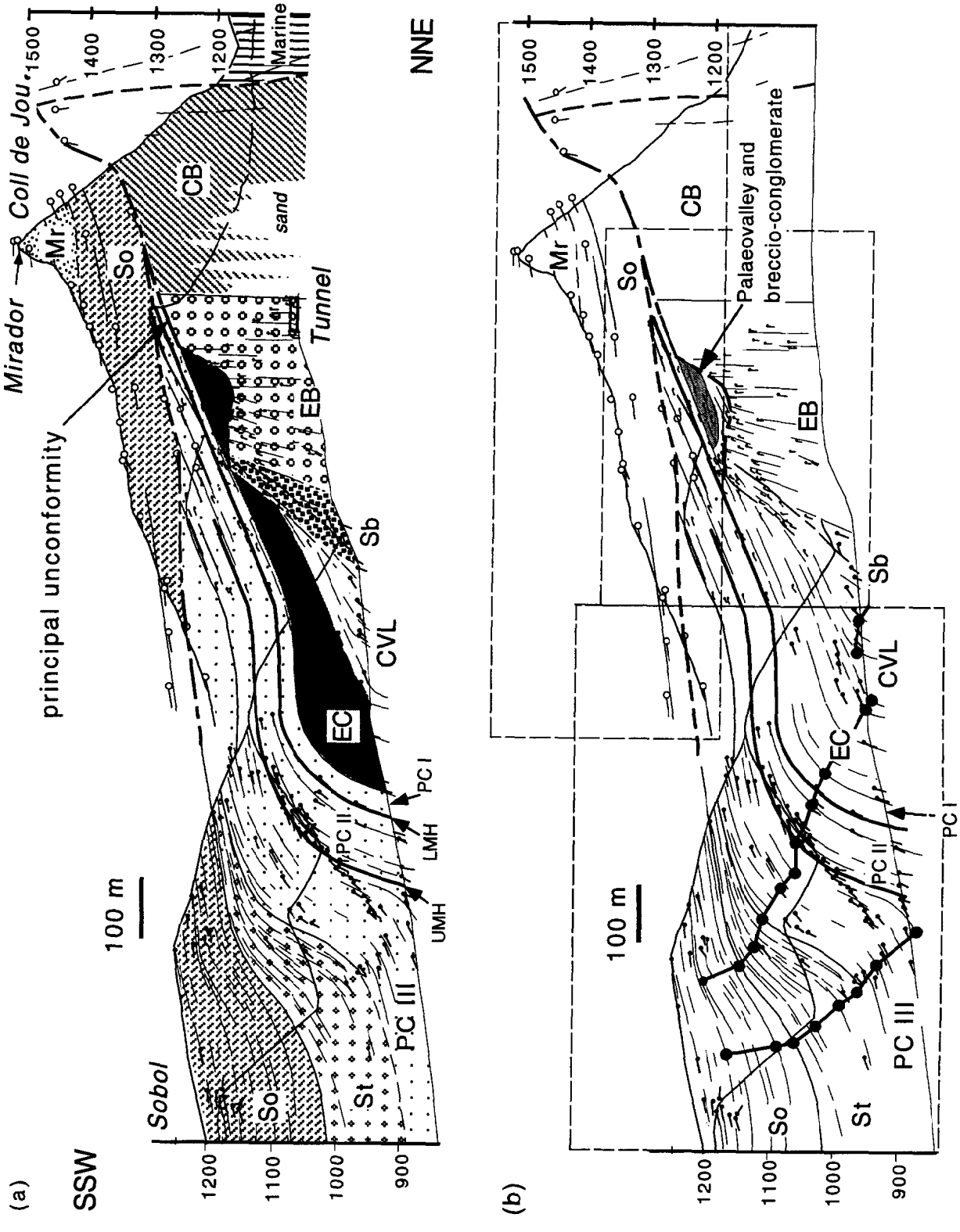


Fig. 7. (a) Profile 1 (Val de Llord) viewed toward the west showing stratigraphy keyed in Fig. 4. Bedding dips are represented by the lollipop symbols. (b) Profile 1 line drawing showing the hinge points for the growth anticline and syncline. These points have been joined to give the growth axial surfaces. Upper and lower marker horizons in black. The section is a composite of three segments (boxes in b) as shown in Fig. 5. *The principal unconformity records major erosion, including a 50 m deep palaeovalley.*

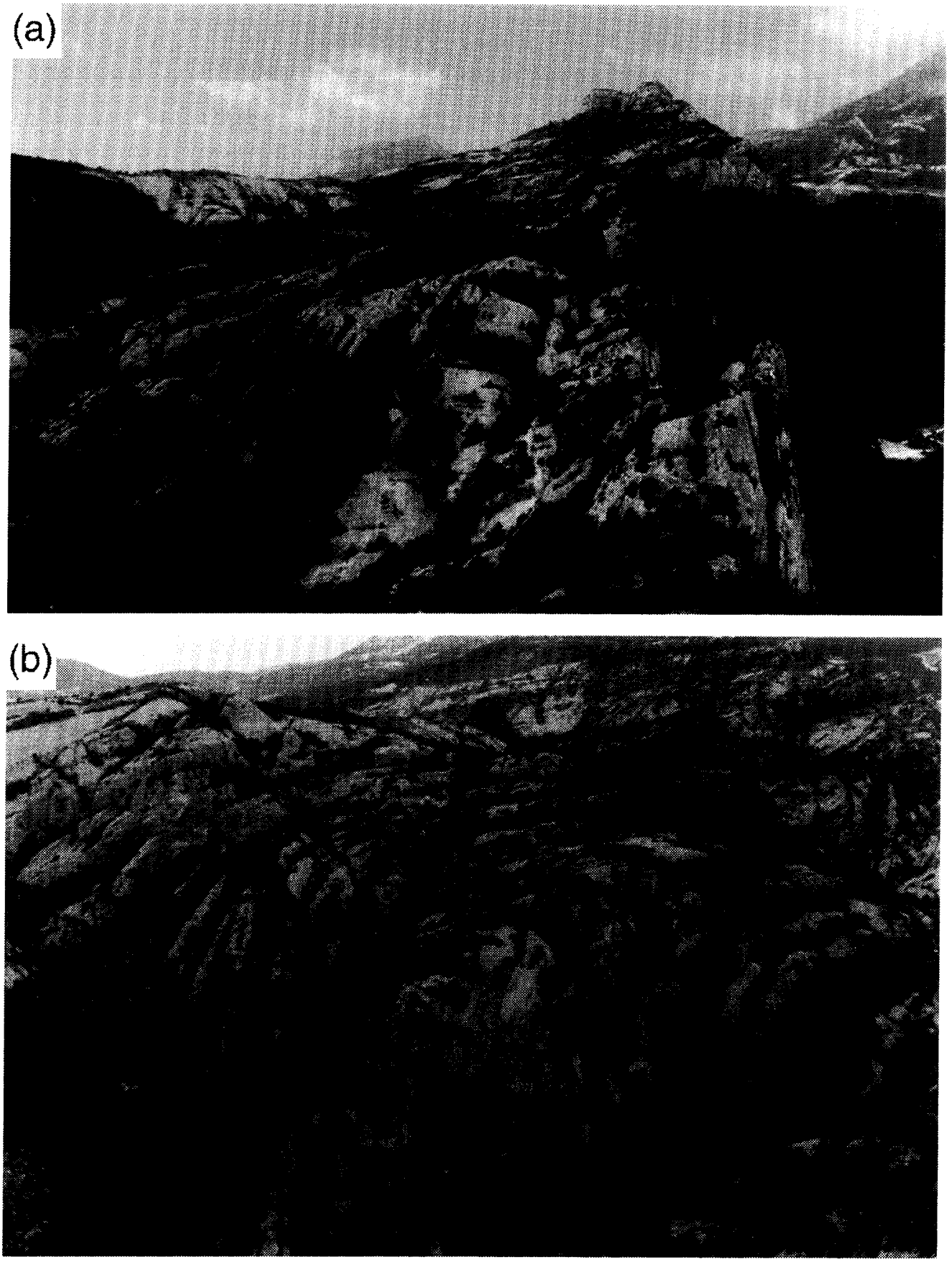


Fig. 8. (a) Photograph looking west at the NW cliffs of Val de Llord, shown on the northern half of profile 1 (Fig. 7). (b) Oblique view toward the NW (taken from the Santuari de Llord) of the growth anticline and syncline on the western side of Val de Llord. Sobol plateau (Fig. 5) in the foreground in the top left hand corner.

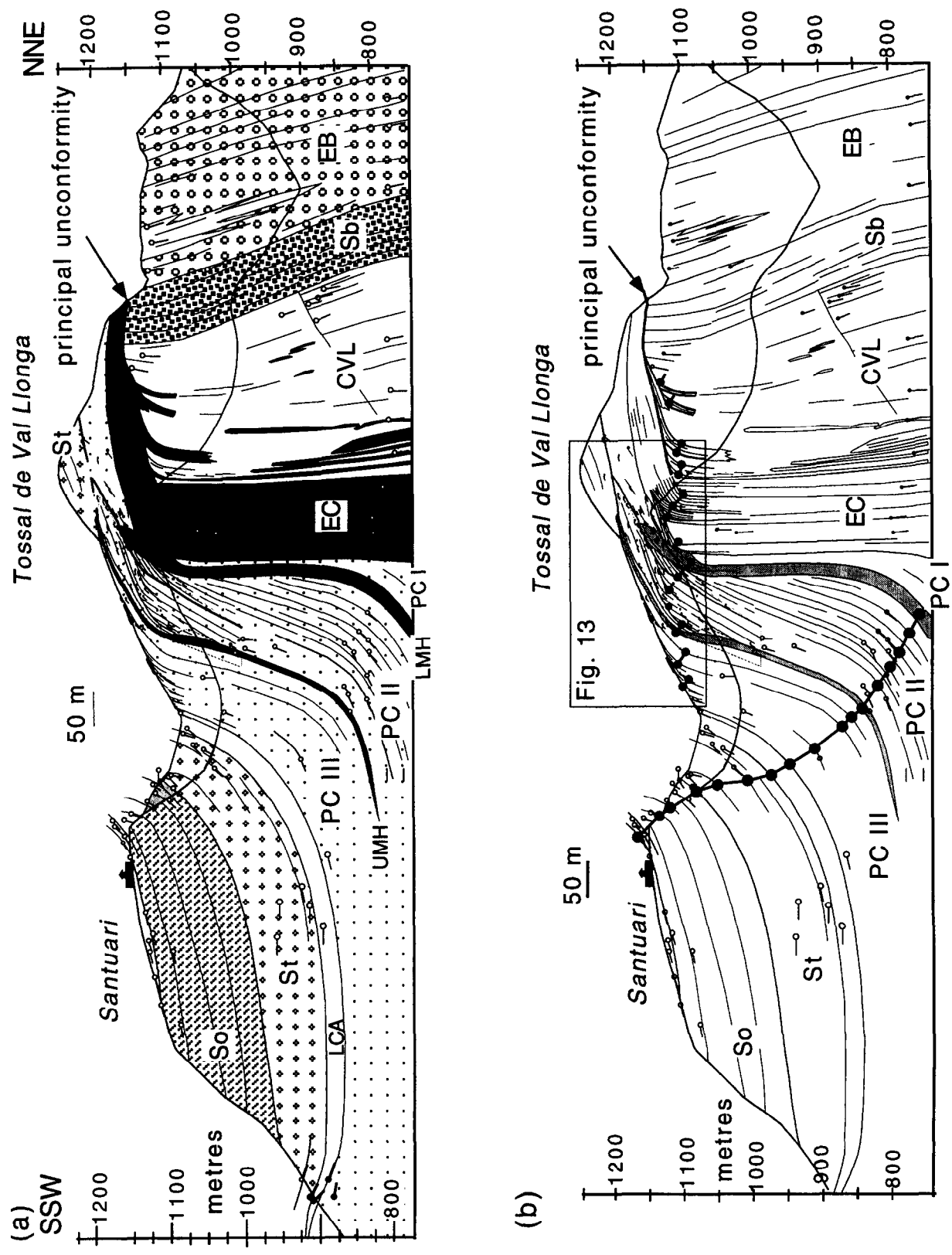


Fig. 9. (a) Profile 2 (Santuari de Llord–Tossal de Val-Llonga) viewed toward the west showing stratigraphy keyed in Fig. 4. The section line is shown on Fig. 5. Corrected bedding data are represented by the lollipop symbols. (b) Profile 2 line drawing with hinge points plotted for the growth anticline and syncline. Upper and lower marker horizons are shaded. The topography of local composite sections is shown superimposed.

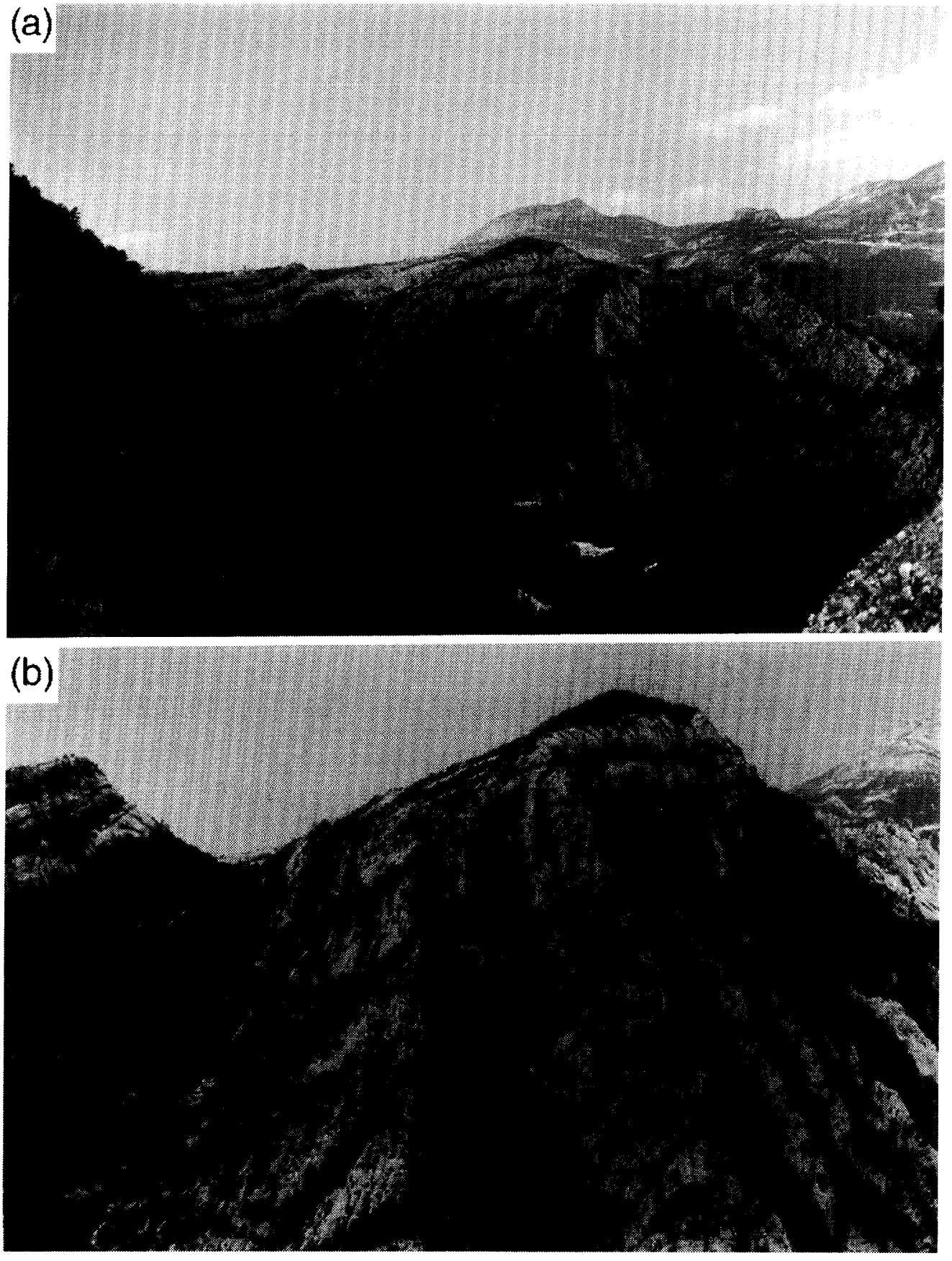


Fig. 10. (a) Photograph of a westward view across Val-Llonga showing the eastern side of Tossal de Val-Llonga roughly equating with profile 2. The monastery Santuari de Lord sits on the plateau to the south. The mirador featured on profile 1 is seen in the background to the north. (b) Westward view of the south-eastern slopes of Tossal de Val-Llonga showing the complex growth geometries within the anticlinal hinge.

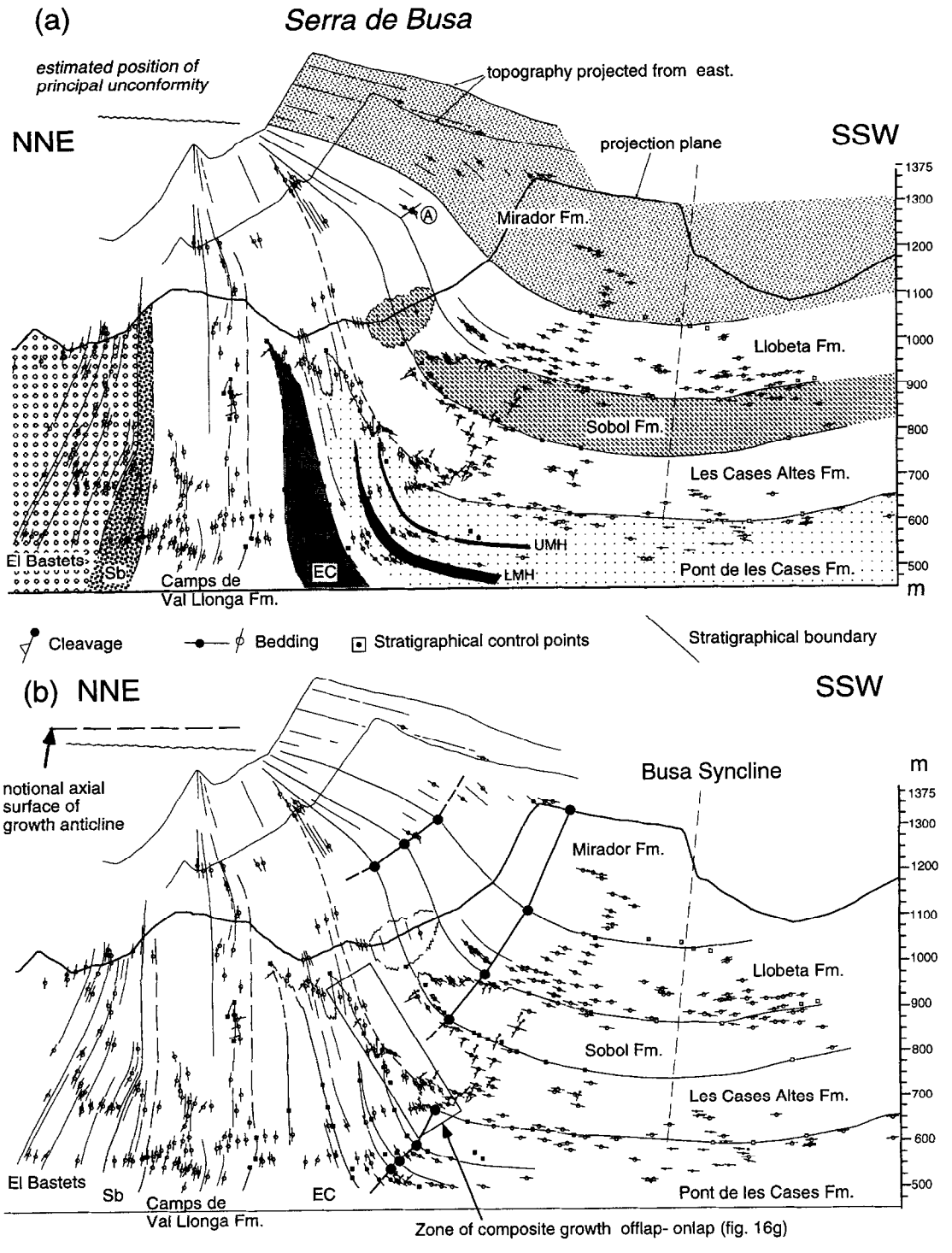


Fig. 11. (a) Profile 3 through the western scarp of Serra de Busa viewed toward the east (see Fig. 5 for location). Key to stratigraphy is shown in Fig. 4. Orientation data have been projected from ≤2 km. (b) Line drawing of profile 3 showing the hinge points for principal stratigraphical horizons and the main unconformities. The hinge points have been joined to give the growth synclinal and anticlinal axial surfaces. Vertical scale is altitude (m) for the topography of the projection plane and does not relate to topography projected from the east.

and many minor unconformities. On the northern side of profile 1 (Figs 7 & 8a) two growth unconformities are visible. The principal growth unconformity separates vertical to overturned strata from an overlying panel of shallowly south-dipping strata (Fig. 7). The erosion represented by this unconformity is significant, including an approximately 50 m deep palaeovalley. To the south of this feature the principal unconformity is difficult to trace as it dips downward into a complex zone which may represent a composite zone of growth offlap–onlap (Fig.

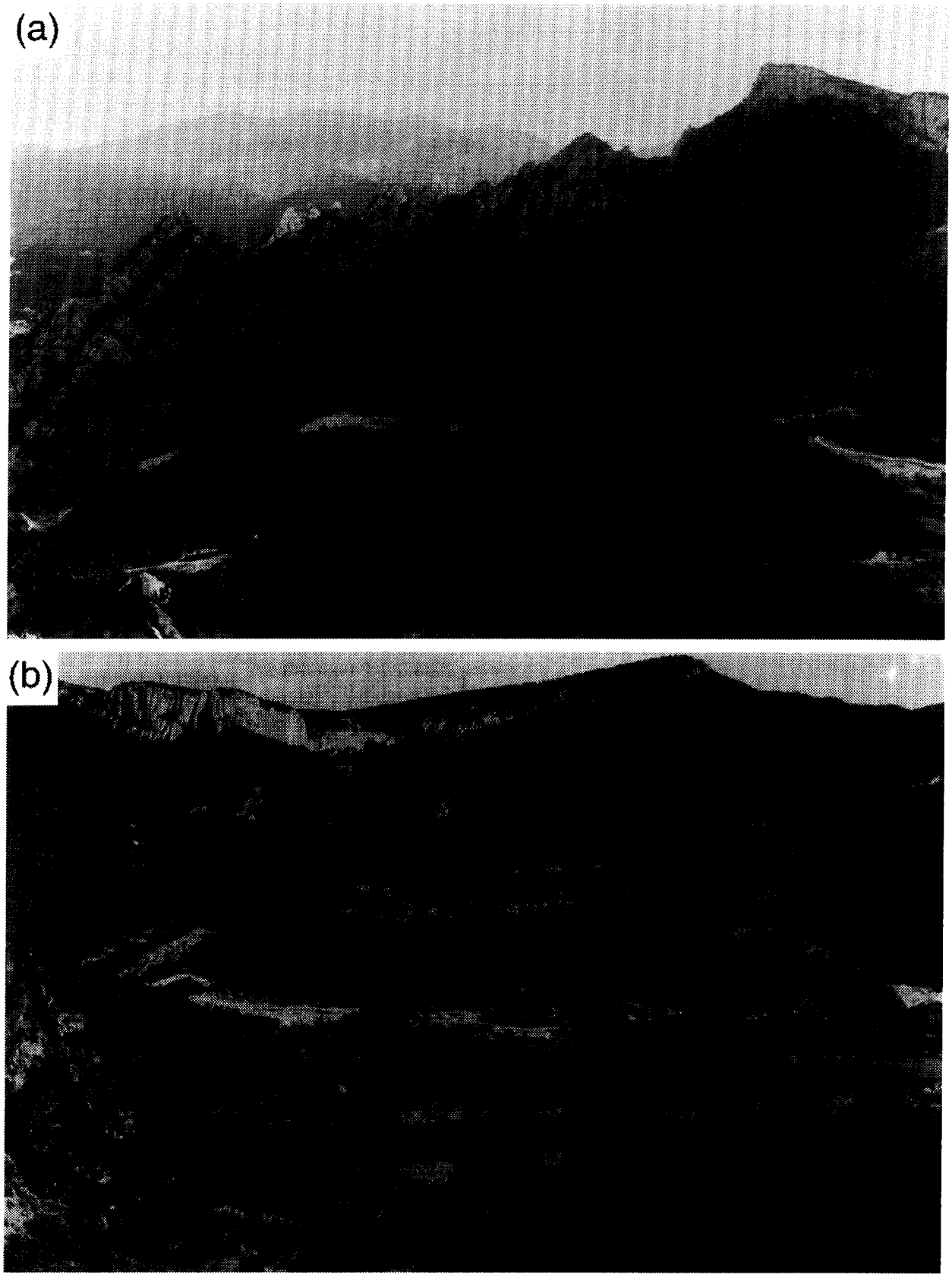


Fig. 12. (a) Photograph of an eastward view towards Serra de Busa showing the northern half of profile 3. Note the synclinal closure in the lower southern foreground. The photograph, taken in July 1995, shows the scar of an access road to a dam which will cause flooding of the Alt Cardener valley (foreground) in the next 3 years, obscuring much of the structure. (b) Eastward view of the southern part of the western slopes of Serra de Busa (Profile 3) showing the closure of the growth syncline in the foreground. The open upright Busa Syncline lies to the south.

16g). Above this level the upper El Castell Formation progressively onlaps and eventually overlaps the erosion surface and infills the palaeovalley (along with a locally deposited breccia–conglomerate unit). The second growth unconformity lies at the base of the Sobol Formation and records a significant tilting (folding) and erosion of the upper limb of the anticline. This erosional surface becomes bedding parallel to the south (Fig. 7a) and it is probable that it developed during deposition of the Santuari Formation which shows strong wedging. Within the fold pair there are no major unconformable surfaces above the Camps de Val-Llonga Formation (Fig. 7a) and all units show a gradual northward thinning and overlap.

The principal growth unconformity can be traced eastward across Val de Llord and around the northern cliffs of Tossal de Val-Llonga (Fig. 5). On profile 2 (Figs 9a & 10) it separates vertical to overturned beds from overlapping units of the El Castell and Pont de les Cases Formations. The principal unconformity partially truncates the tops of anticlinal closures in the Camps de Val-Llonga Formation (Fig. 9b). Smaller internal growth unconformities curve upward to merge into the main surface making this a composite growth unconformity. The main surface abruptly becomes bedding parallel within the El Castell Formation. In comparison to profile 1, the downcutting along the unconformity in this area is minor suggesting a stronger erosion to the west.

On profile 2 the El Castell Formation, and particularly the Pont de la Cases Formation, show notable thickening southward across the anticline (Figs 9, 10, 13 & 14). Changing geometries in the hinge zone indicate that the ratio of erosion to sedimentation changed through time on various scales. The lower marker horizon onlaps (abuts) a 50 m high palaeocliff caused by a major local erosional event (Fig. 13). Two other incision–onlap events of similar magnitude occured in quick succession in Member 2 of the Pont de les Cases Formation (Fig. 13). On the larger scale, succeeding strata overlapped the anticline (Figs 9 & 13) suggesting that the gross sedimentation rate became greater than uplift rate. However, on a smaller scale, packages recording sequences of offlap–(incision)–onlap–overlap can be seen. The upper member of the Pont de les Cases Formation records growth offlap.

The principal unconformity and much of the growth anticline have been eroded on profile 3 (Fig. 11). This section is however particularly valuable for the analysis of the stratigraphic geometries of the growth syncline that are not well exposed in the other two profiles. Substantial thickening of stratigraphical units occurs southward across the growth syncline (Fig. 11a) and within the steep limb the strata also thin markedly upward. In the core of the syncline the Pont de les Cases Formation (particularly Member 3) records growth offlap, followed by local growth onlap of the overlying Les Cases Altes Sandstone Formation (Fig. 11b, boxed area and Fig. 12b, lower left hand corner). This produces the complex of fanning dips which can be followed along the boundary between these two units in the core of the syncline (Figs 11b & 16g). The upper Les Cases Altes Sandstone Formation displays an apical wedge (Fig. 16d). Younger formations show wedging and growth overlap indicating that in this eastern region the fold

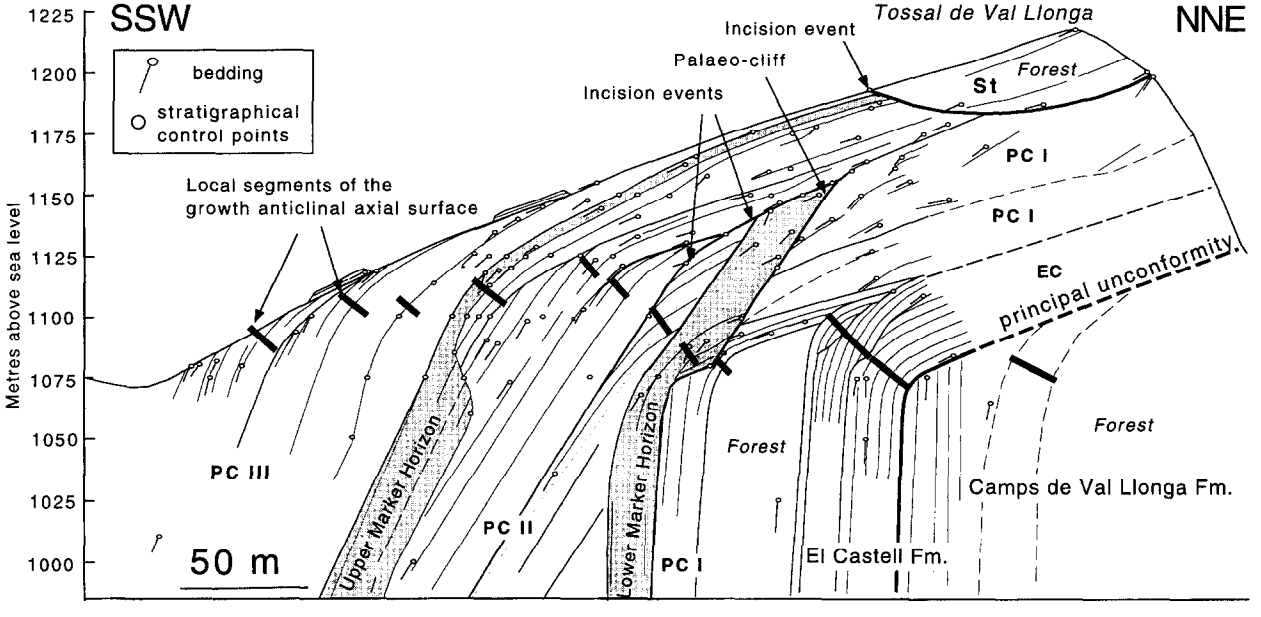


Fig. 13. Detailed profile through the Tossal de Val-Llonga, based on 1:1250 mapping, showing depositional geometries across the growth anticlinal hinge (located on Fig. 9b). The hinge points of depositional surfaces can only be joined to form an axial surface for short segments. These segments form an en échelon pattern, stepping downward up-section across the anticlinal closure. The main internal unconformities are shown by heavy lines. Locally measured and projected bedding data have been corrected for apparent dip.

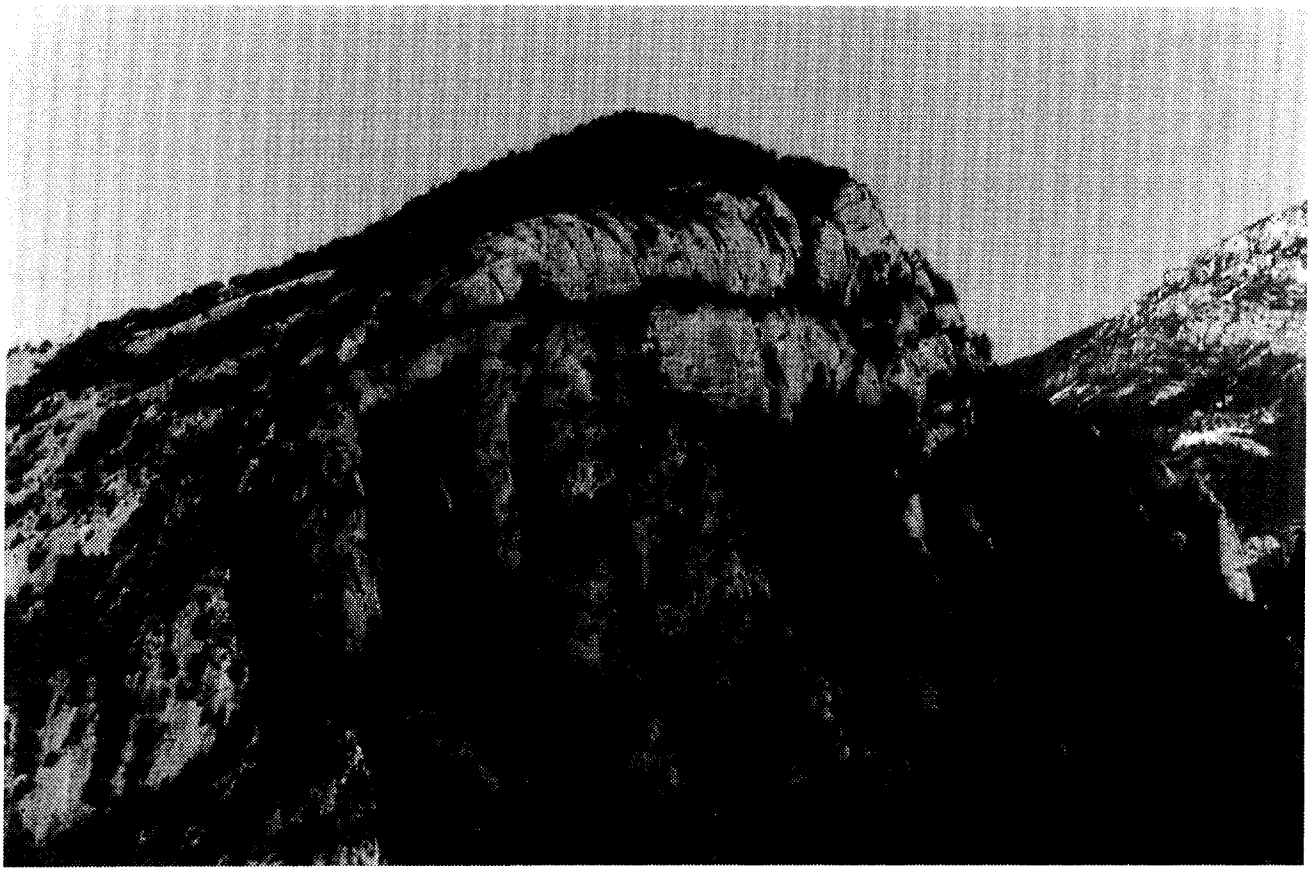

Fig. 14. Photograph of the southeastern slopes of Tossal de Val-Llonga showing the exposure of structures represented in Fig. 13.

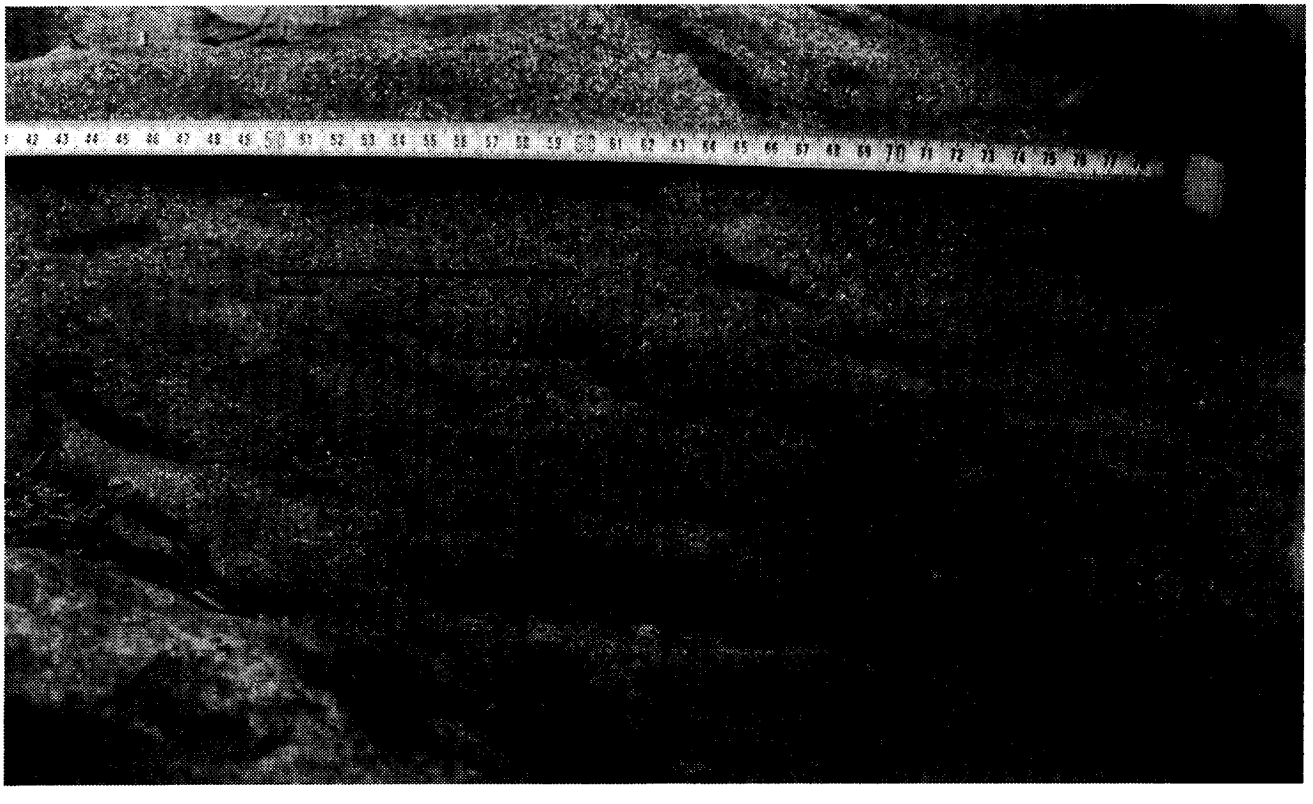

Fig. 15. Northward view of a south-dipping upper bedding plane in a sandstone from the growth syncline hinge in the river bed of the Alt Cardener. Pressure solution cleavage traces are well developed and associated with elliptical cross-sections through burrows which record cleavage strain. Scale in centimetres.

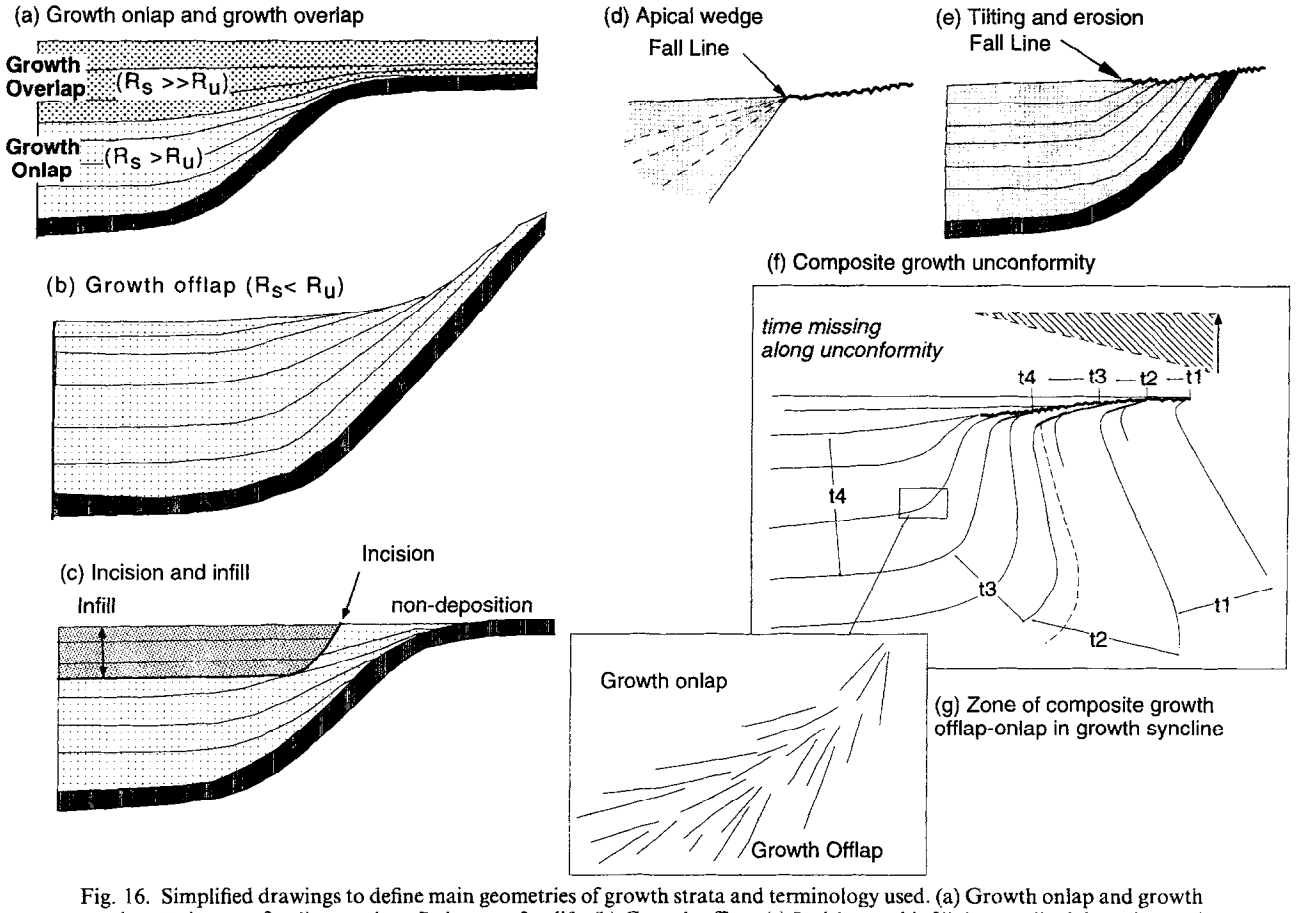


Fig. 16. Simplified drawings to define main geometries of growth strata and terminology used. (a) Growth onlap and growth overlap; $R_s$ is rate of sedimentation, $R_u$ is rate of uplift. (b) Growth offlap. (c) Incision and infill due to alluvial erosion and deposition. Incision can be symmetrical to give a palaeovalley such as that seen on profile 1. (d) Apical wedge. (e) Tilting and erosion. (f) Composite growth unconformity, t1–t4 represent time steps in the development of the growth unconformity. (g) Zone of composite growth offlap–growth onlap in growth syncline.

structure continued to develop after growth had ended further west.

## MESOSTRUCTURES

Analysis and distribution of minor structures within the growth strata provide insights into the strain history at different levels of the structure, which in turn has implications for the folding mechanism and kinematics. The principal minor structures consist of cleavage, minor faults and bedding-parallel slip surfaces.

### *Cleavage*

A weak to moderate pressure solution cleavage is found in sandstone beds mainly in the hinge zone of the growth syncline (Figs 11 & 15) in the eastern regions, but also intermittently in the steep panel. The cleavage is present at all stratigraphic levels in the fold hinge, but is most strongly developed in the oldest sandstone lithologies. Associated conglomerates do not contain mesoscopic planar or clast-shape fabrics indicative of significant strain. Poles to cleavage plot as a loose cluster and give a mean cleavage plane of 091/52°N (Fig. 6f). This, together with fold orientation data, indicates a 10° anticlockwise (ACW) axial cleavage transaction (Johnson, 1991) for the whole of the structure, and 14° ACW for the growth syncline in the south-east.

The presence of cleavage almost exclusively in the syncline indicates that the hinge was fixed in these rocks and progressively tightened as the growth fold developed. Such a systematic ACW transecting relationship can be interpreted to record fold amplification in a regime of weak sinistral transpression (Soper, 1986).

### *Mesofractures*

Minor faults with relatively small displacements (<0.5 m) are most intensely developed in the overturned to vertical marine and continental strata (Fig. 17). The density of faulting decreases southward towards the younger, less inclined strata. Both reverse and less significant strike-slip faults are commonly developed in conjugate sets. The reverse fault set achieves minor dip-parallel extension while the strike-slip faults record minor strike-parallel extension (Fig. 18). Together, these small faults accommodate northward-intensifying tectonic

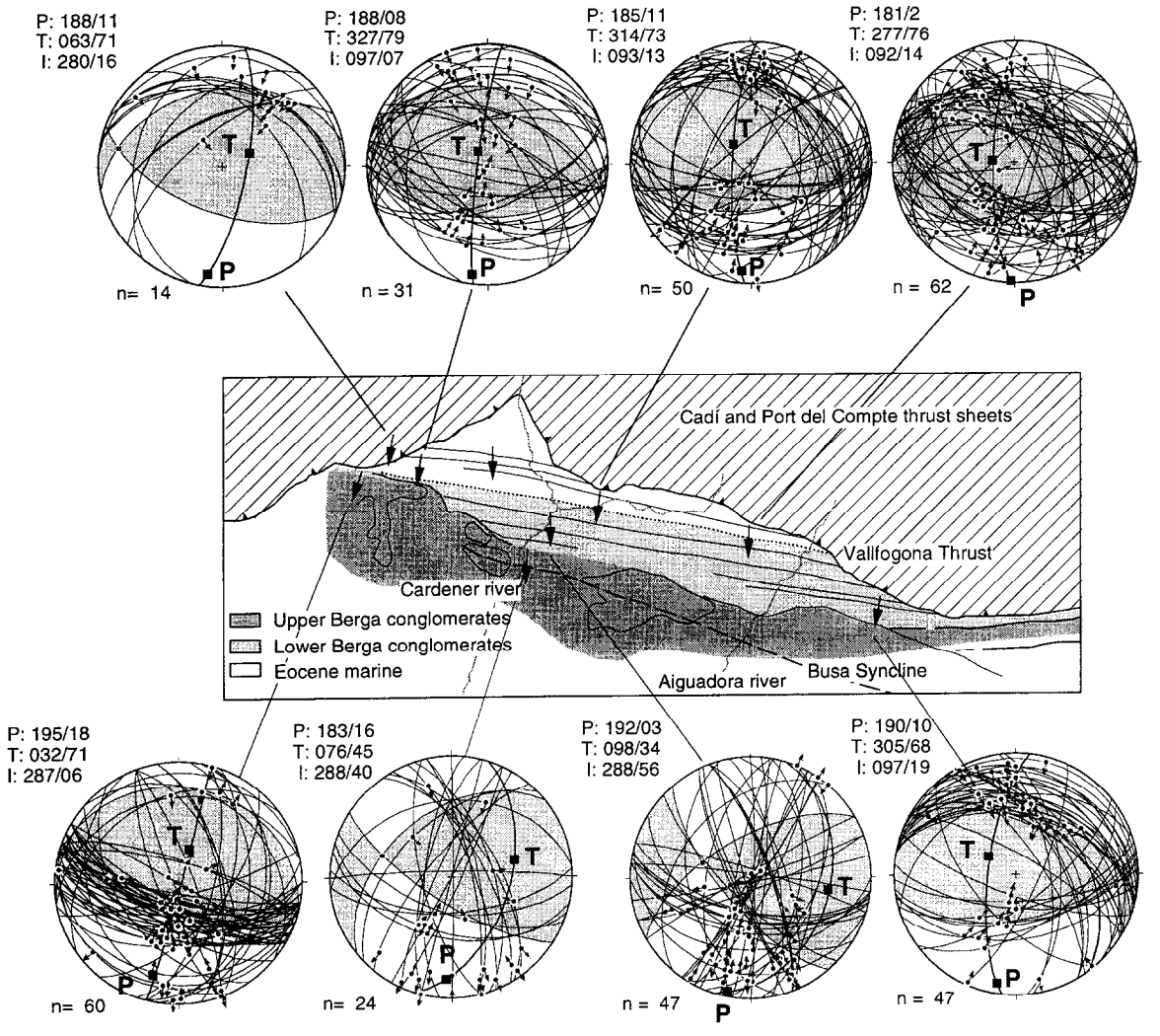


Fig. 17. Fault planes and slip vectors from homogenous sub-areas plotted on lower hemisphere equal area stereonets. The palaeostress axes are derived for each sub-area using the program FaultKin (version 3.8a, Allmendinger *et al.*, 1994). *P*, compressional axis; *T*, tensional axis; *I*, intermediate axis; *n*, number of data. The *P* axis trend for each locality is represented by an arrow on the map.

thinning of the steep beds. The conjugate reverse faults show no preferred cross-cutting relationship, indicating a synchronous development. In vertical beds south-directed reverse faults show a gentle ($\approx 20°$) north dip whereas south-dipping reverse faults are steeper ($\approx 35°$) thus giving a south-plunging acute bisector (*P*-axis, Fig. 17). The apparent tilting of the conjugate reverse faults suggests that they formed in already steeply dipping beds, and were then rotated as the beds steepened further.

A regional analysis of fault kinematics was made by grouping data into homogeneous stratigraphical and tectonic localities to calculate mean palaeostress orientations (Fig. 17). Initially, south- and north-directed reverse faults as well as strike-slip faults from the same locality were analysed separately. The coherence of these results allow us to present all the measurements from a single locality together (Fig. 17). The fault kinematic analyses show that: (1) The direction of compression for the whole area was 187°. There was no appreciable change in this orientation either along strike or up-section (through time). Thus all these structures can be interpreted to have formed during a single, continuous period of deformation. (2) Compressional faults in both the hangingwall and footwall of the Vallfogona thrust are related to the same stress field. Thus the Vallfogona thrust was emplaced during fold growth. (3) Bedding-parallel top-to-south slip in the youngest, sub-horizontal conglomerates directly below the Vallfogona thrust at the Coll de Jou (Fig. 5) record footwall deformation during the emplacement of the thrust sheet (Fig. 18).

Calcite slickenfibres on planes parallel to bedding lie consistently down-dip in the steep to overturned panel (Fig. 18). The occurrence of these surfaces decreases southward. Where no well-developed bedding is present in the conglomerates, slip surfaces appear to be new

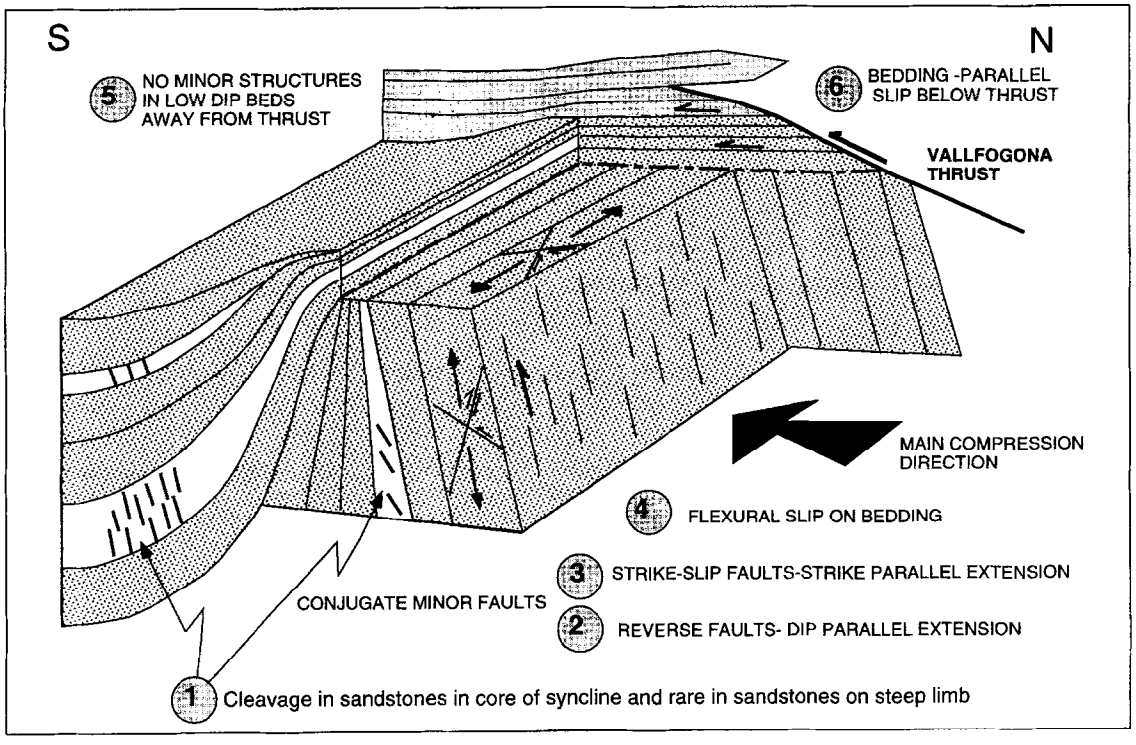


Fig. 18. Simplified three dimensional cartoon of the Sant Llorenç de Morunys structure showing the distribution of mesostructures.

fractures. Some sandstone beds record dip-parallel slip by brecciation and minor fault development. All bedding-parallel slip surfaces give a slip sense which is compatible with flexural slip folding. Internal deformation of the conglomerates is recorded by the common presence of shear vein fibres wrapping large clasts, coupled with directional pitting (Schrader, 1988).

These mesostructural data indicate that internal deformation of the Berga Conglomerate Group was progressive and ongoing at all stratigraphical levels during development of the growth structure (Fig. 18). The older and steeper beds show the most intense deformation. No minor structures are found in the hinge of the growth anticline, indicating that in these unconsolidated sediments folding was accommodated largely by intergranular slip.

Compressional axes derived from cleavage and minor fault analyses (Figs 6f & 17) are 13° and 7° anticlockwise, respectively of the compression direction derived from the mean fold axis (Fig. 6a). These observations support the proposal that folding evolved within a weak sinistrally transpressive regime.

## SEQUENTIAL RESTORATION

### *Procedure*

The three profiles were restored in up to eight steps related to stratigraphical units (t1–t8, indicated in Fig. 4) to the base of the El Castell Formation in order to examine the progressive development of the growth fold (four steps are illustrated in Fig. 19). The restoration technique adopted avoids prior assumptions of fold mechanism by utilising, as far as possible, the basic principles of section balancing (Dahlstrom, 1969; Hossack, 1979). The assumptions and techniques used here and their validity for this study area are discussed below.

(1) Successively older stratigraphical boundaries, which approximate bedding, are restored to horizontal. No evidence has been found for strongly inclined depositional surfaces and away from the growth anticline major contacts are parallel to stratification above and below in most cases. This indicates very low inclinations of depositional surfaces. Inclinations of alluvial fan radial surfaces are between 2° and 13° (mode 4–5°), and those of longitudinal profiles in boulder to cobble grade rivers are 0.25° (Blair and McPherson, 1994). Therefore, assumption of originally horizontal strata may, at worst, produce a slight distortion due to over-restoration.

(2) The cornerstone of the restoration procedure is the assumption that bed length is preserved. Along with preservation of thickness, this leads to the conservation of volume during deformation and growth. Through the steps of the sequential restoration individual particles in a bed will thus describe an arcuate path (restoration vector) about the pin line of the bed (Fig. 19).

(3) Thickness of major stratigraphical units is

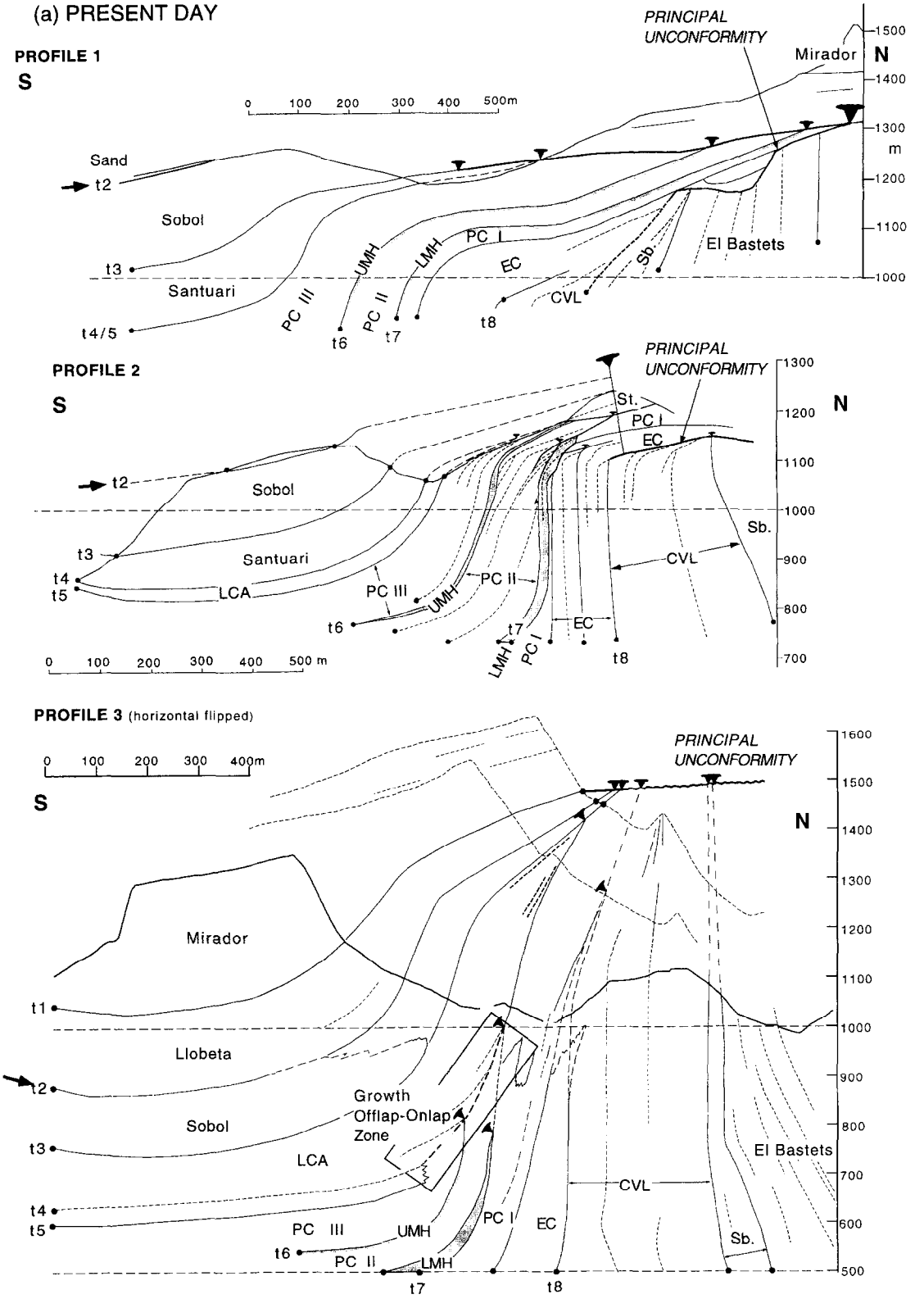


Fig. 19. Sequential restorations of the three profiles. (a) Simplified present-day profiles showing hinterland pin-points for each stratigraphic boundary (profile 3 is shown as a mirror image of Fig. 11 for comparative purposes). Arrows indicate the level to be restored in the next step. Key to stratigraphical abbreviations in Fig. 4. Sections were restored in up to eight steps representing different stratigraphic levels, t1 to t8, as shown here. Only four of the steps are shown in (b) to (d).

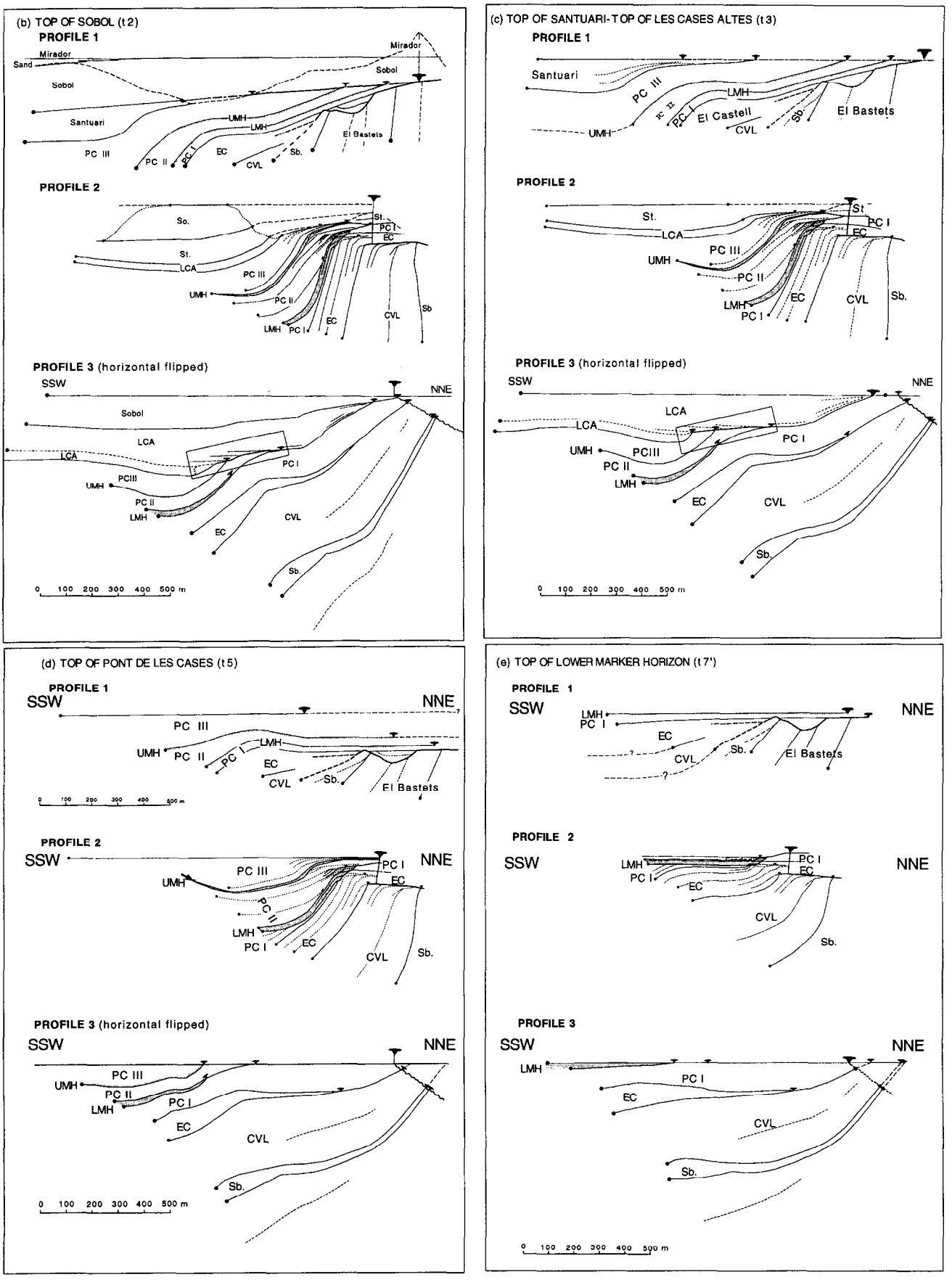


Fig. 19. *Continued.*

preserved as far as possible. By definition, growth folds affect unlithified to semi-consolidated sediments. Depending on lithology, progressive compaction can cause a significant decrease in volume. However, in this area coarse conglomerates preserve primary depositional fabrics (e.g. imbrication) showing that they have not undergone significant compaction (Hails, 1976). During folding, strain-related thickening can occur in fold hinges, whereas on fold limbs thickening followed by thinning can occur in beds as they rotate through to overturned positions. As described above, evidence for these types of fold-related strain is found in this region, but strain levels are low and therefore, on the scale of the cross-sections, do not significantly affect bed-length or thickness.

(4) Individual horizons on each section are pinned in the hinterland. A pin-line can be drawn perpendicular to the upper limb of the growth anticline for the upper formations on profile 1 (Mirador and Sobol Formations) and on profile 2 (above and including the El Castell Formation). Individual horizons below these levels are pinned at their intersection with the overlying unconformities. On profile 3 pin-points are drawn at the projected intersection of steep horizons with the inferred position of the principal unconformity (Fig. 19a), and at offlap points within the steep shared limb of the fold pair. These pin-points were chosen because (1) there is no evidence of slip transfer across observed unconformities or of fold-related slip above the anticlinal hinge; and (2) earlier attempted restorations with foreland-located pin-lines generated unacceptable distortions of the growth fold geometry. Beds intersecting upward with growth unconformities can therefore only be pinned at these points. This method has been developed specifically for detailed restoration of growth folds. As the profiles cannot be pinned in the foreland, area cannot be constrained. Loose lines (Marshak and Woodward, 1988), drawn perpendicular to bedding at the last control point on the base of each stratigraphical unit on the foreland side, were used to monitor distortion through the folding stages. Most loose lines (not shown) become stretched and sheared as units pass from horizontal into the steep limb.

*Results I: three-dimensional geohistory*

We distinguish four periods of fold development related to the relative rates of sedimentation ($R_s$) and fold growth (uplift, $R_u$). The geometries produced by the restoration become successively less well constrained back through time.

*Period 1.* Before deposition of the Sobirana Formation, available data suggest that the growing fold pair evolved steadily as it migrated southward, with the level of erosion fluctuating close to the level of the anticlinal closure. This implies that $R_s$ was equal or slightly less than $R_u$. In the west (profile 1) the level of erosion was deeper with respect to the anticlinal closure. During deposition of the Sobirana Formation apparent offlap indicates that $R_s/R_u$ gradually decreased in the west. This effect cannot be detected on profiles 2 and 3.

*Period 2.* On profile 1, onlapping geometries in the Camps de Val-Llonga and the El Castell Formations record a subsequent increase in $R_s/R_u$. The El Castell Formation (Fig. 19e) eventually overlapped the principal unconformity north of the growth anticline. On profile 2, an increase in $R_s/R_u$ is also indicated first by the preservation of anticlinal closures below the principal unconformity in the Camps de Val-Llonga Formation. The El Castell Formation then overlapped the anticlinal closure. This formation shows considerable thickening and numerous internal unconformities across the anticlinal closure, suggesting that fold growth was greater toward the east. The anticlinal closure for this stratigraphical level is not seen on profile 3.

*Period 3.* The Pont de les Cases Formation records the most complex phase of fold development on all the profiles (Fig. 19d). In the west (profile 1) sedimentation continued to overlap the gently growing fold pair with little wedging ($R_s/R_u$ was high and constant). Further east (on profile 2), increased fold size provided more accommodation space in which a thicker Pont de les Cases Formation accumulated. The lower marker horizon and the lower beds of Member 2 record prolonged periods of fluvial erosion localised on the growth anticline hinge. Short periodicity $R_s/R_u$ variations were superimposed on a long time-scale increase in $R_s/R_u$ in the middle levels of this formation. Growth offlap dominated in the upper member ($R_s/R_u$ decreased). A 25 m deep incision on Tossal de Val-Llonga (Fig. 13) may have occurred synchronously or following this period of growth offlap. On profile 3, the Pont de les Cases Formation is not significantly thicker than on profile 2 in the core of the syncline. Above the lower marker horizon the formation records growth offlap within the synclinal core due to a decrease in $R_s/R_u$.

*Period 4.* Above the Pont de les Cases Formation all profiles are dominated by growth overlap (Fig. 19b & c). Clearly, the sedimentation rate everywhere became greater relative to fold growth rate. On profile 1, the upper limb of the anticline was tilted and eroded ($R_s/R_u$ decreased) during deposition of the Santuari Formation which tapered strongly across the fold pair. The following Sobol and Mirador Formations overlapped the entire area to the west and show little evidence of growth. On profile 2 the Santuari Formation overlapped northward, showing some growth. The geometries of younger units are not preserved. On profile 3 the lower beds of the Les Cases Altes Formation show growth onlap (Fig. 16g) across the top of the Pont de les Cases Formation in the hinge of the growth syncline (Fig. 11b) while upper beds formed an apical wedge. Overlying formations show growth overlap continuing into the

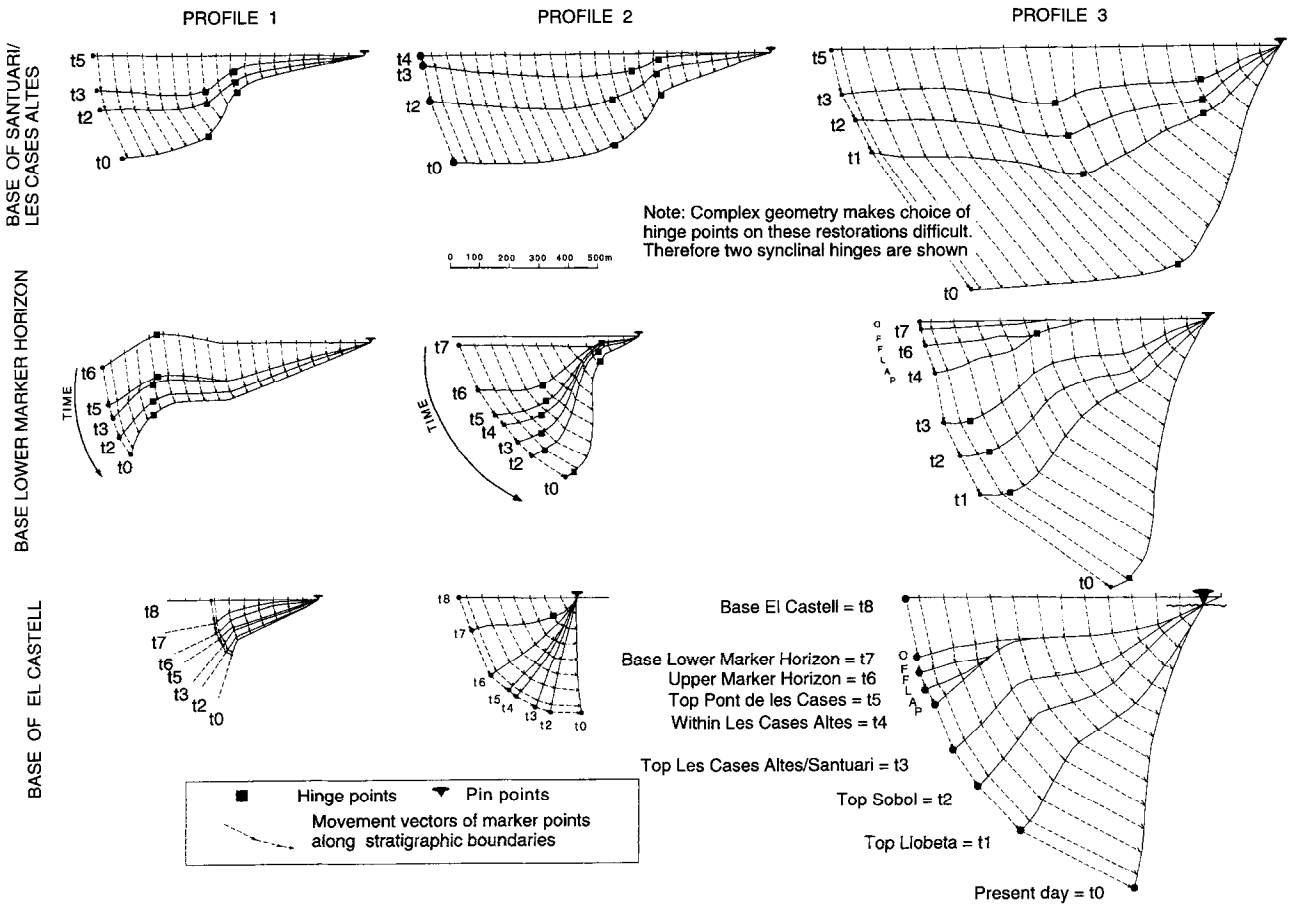


Fig. 20. Progressive folding paths of three stratigraphic horizons (observed portions only) on each of the three profiles. The folding paths, tracked from horizontal to present day, are derived by sequential restoration (Fig. 19). Each step represents the position of the *tracked horizon* when the named horizon (t0–t8) was horizontal. Up to eight steps are shown (keyed in lower right hand corner). Hinge points for the growth anticline and syncline are shown (squares) where possible for each restoration step; limb rotation was accompanied by a minor component of hinge migration due to deposition of wedge-shaped units. Dashed lines represent the movement vectors of marker points on the selected stratigraphical horizons. These all follow curved rotational paths around the pin-point.

uppermost levels of the Mirador Formation. These relationships suggest that in this eastern area both fold growth and sedimentation rates continued to be high while further west folding died out and local development of accommodation space was reduced.

### *Results II: mechanisms and kinematics of fold growth*

Figure 20 shows the progressive folding paths of three stratigraphic horizons on each of the three profiles, derived from sequential restoration as described above. Clearly, the fold pair grew more rapidly and for a longer period in the east (profile 3) accommodating a thicker sedimentary sequence in the syncline. The dashed lines, representing movement vectors of marker points on the stratigraphical horizons, follow curved paths about the pin-point, recording fold growth principally by limb rotation. Up to eight steps (t1–t8) are shown. Hinge points for the growth anticline and syncline are shown where possible for each restoration step and demonstrate that limb rotation was accompanied by minor passive hinge migration through time. The hinges of both folds tended to migrate toward the foreland but the synclinal hinge point migrated more than the anticline. This is a geometrical phenomenon (Ramsay, 1967) of growth folding, due to the progressive addition and folding of wedge-shaped sedimentary bodies. This is emphasised by the major hinge point jumps associated with periods of offlap (e.g. t5–t7 on profiles 2 and 3). Such passive hinge migration is a unique phenomenon of growth folds and would not occur in folding of non-growth strata.

## NUMERICAL MODELLING

As argued earlier, regional evidence suggests that the Sant Llorenç de Morunys structure is neither a detachment nor a fault-bend fold (Vergés, 1993). This discussion will therefore focus on the applicability of three contrasting numerical models of fault-propagation fold-

ing to the geometries observed in profiles 1–3 (Figs 7, 9 & 11): the fixed-axis and constant-thickness models of Suppe and Medwedeff (1990) and the trishear fault-propagation fold model of Erslev (1991). These models predict fundamentally different kinematics of fold growth. The models of Suppe and Medwedeff (1990) assume kink band formation and limb lengthening while the model of Erslev (1991) incorporates distributed deformation in a triangular shear zone and non-rigid limb rotation (Fig. 1).

*Modelling methods*

The models presented in this section have been developed using a finite difference modelling approach described previously by Waltham and Hardy (1995). The tectonic deformation of a geological surface is modelled using a velocity description of deformation, while background sedimentation and local erosion, transport and sedimentation are modelled for the top surface. An Eulerian finite difference scheme is needed for the combination of deformation and sedimentation for the topmost surface, while the deformation of buried surfaces is modelled using a simple Lagrangian scheme. This avoids any numerical diffusion or dispersion and is particularly useful when steep or overturned surfaces are developed as a result of deformation. Hardy and Poblet (1995) provide a detailed discussion of this method applied to compressional growth structures.

*Sedimentation.* In each model sedimentation can be the result of two distinct processes: (1) background sedimentation and (2) local erosion, transport and deposition. Background sedimentation is considered to be a non-locally sourced sedimentation rate, which occurs everywhere below a specified base level. Local erosion, transport and sedimentation are modelled using a diffusion mechanism in which sediment flux is proportional to local slope. The diffusion model results in material being eroded and transported away from any steep slopes which develop during a model run. This is appropriate in general to the Sant Llorenç de Morunys structure, as the bulk of the sediment was derived from south-east Pyrenean thrust sheets and the axial zone, whereas local structurally-developed relief created local source areas.

*Fixed axis and constant thickness fault-propagation folding.* The details of these models are given in Suppe and Medwedeff (1990) and Mosar and Suppe (1992), and a velocity description of deformation is given in Hardy and Poblet (1995). The fundamental process by which folds grow in these models is by kink band formation and migration. Active synclinal axial surfaces, across which particles move during fold growth, are fixed to the footwall where the fault steps up from the décollement and to the fault tip (Fig. 21a & b). Limbs lengthen through time but do not rigidly rotate and the fold grows self-similarly. For a simple step-up fixed-axis fault-propagation fold, forelimb thickening occurs at angles less than 29° while forelimb thinning occurs at greater angles. For step-up angles in the range 10–40° the magnitude of this thickening or thinning can be up to 40%. As the dip of the ramp decreases the front limb becomes steeper, although it is never overturned.

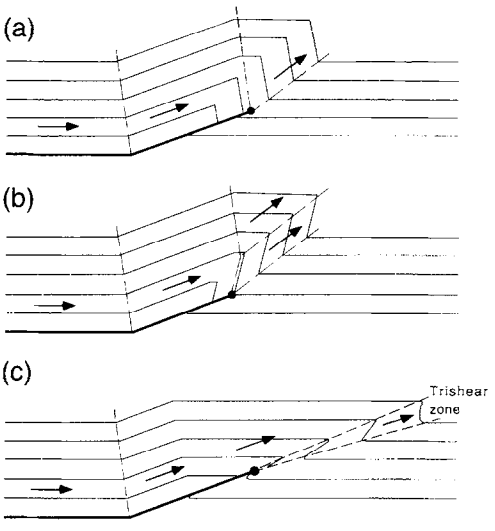


Fig. 21. Illustration of active axial surfaces associated with (a) fixed-axis kink-band and (b) constant-thickness kink-band models. (c) Trishear fault propagation folding model, showing the boundaries of the trishear zone. Ramp (step-up) angle is 20°. Particle displacement directions within each zone are illustrated schematically by arrows.

In the constant thickness fault-propagation fold model, unlike the fixed-axis theory, bed thickness is maintained during fold growth and the geometry of active surfaces is somewhat different (Fig. 21b). For a simple step-up constant thickness fault-propagation fold, overturned forelimbs occur at angles less than around 25°. However, in order to maintain constant bed thickness, this model can have some unlikely geological properties at low step up angles ($<29°$). In these cases material can be incorporated into overturned forelimb beds and then roll onto the crest of the structure.

*Trishear fault-propagation folding.* The basis of the trishear model is given in Erslev (1991) and Erslev and Rogers (1993). The fundamental feature of trishear is distributed deformation in a triangular shear zone attached to a fault tip (Fig. 21c). The original model (Erslev, 1991) did not include a ramp or syntectonic sedimentation. We have added both of these features in order to make the results directly comparable to the kink band fault-propagation models. A more significant modification, however, is the facility to allow variable ratios of fault-tip propagation to fault-slip rates ($p/s$ ratio). In the original model the fault tip either did not propagate at all or propagated at the slip rate (Erslev, 1991; Erslev and Rogers, 1993). This rather artificial restriction is relaxed, as fault-tip propagation is known to exceed slip rate in nature (Williams and Chapman, 1983). In all fixed-axis kink-band models described below

$p/s = 2$ (Suppe *et al.*, 1992); for comparative purposes the same value is used in the trishear models presented. In constant-thickness models the $p/s$ ratio depends upon the step-up angle. In the simple step-up trishear model used here an active axial surface is also present on the back limb (Fig. 21c).

*Characteristic features of growth kink-band and trishear fault-propagation folding*

In order to illustrate the characteristic features of both growth kink-band and trishear fault-propagation folding a series of comparative examples are now investigated. In each case the model parameters are similar so that comparisons between the three models can be made. In all models ramps step up from a flat detachment, and fault slip rate is constant (1.0 m ka$^{-1}$).

In the first case (Fig. 22) the rate of base level rise is high (1.0 m ka$^{-1}$) and is always filled to the top with sediment in order that the upper surface is at all times flat. The models produce quite different growth strata. Firstly, in the kink band models all forelimb beds within regions bounded by axial surfaces have a uniform dip in both the growth and the pre-growth strata (Fig. 22a & b), while forelimb beds in the trishear model show a continuous variation from overturned to steep beds in the pre-growth strata to flat lying strata at the top of the growth sequence (Fig. 22c). Secondly, growth strata produced by the kink band models show changes in thickness only across axial surfaces, and thus within the forelimb growth triangles beds have constant thickness. In the trishear model, growth strata in the forelimb thin toward the crest. Both the fixed-axis and trishear models predict tectonic thickening of pre-growth and growth strata in the forelimb of the structure. Clearly, the trishear model predicts considerable accumulated strain in the shared limb and particularly in the syncline which is expressed as thickening (Fig. 22c). The observed thickening is a combination of growth and tectonic strain. Thirdly, kink band migration models produce folds with angular hinges while the trishear model produces rounded fold hinges. Finally, the growth strata on the back limb of the kink band models show a complex set of growth triangles while those developed in an equivalent position in the trishear model show only a single growth triangle. These features will not be discussed further because no back limb is observed at Sant Llorenç de Morunys because of truncation by the Vallfogona thrust.

In the second example (Fig. 23) all parameters are the same as the previous case except that the base level rise has been reduced. Only the growth strata on the forelimb

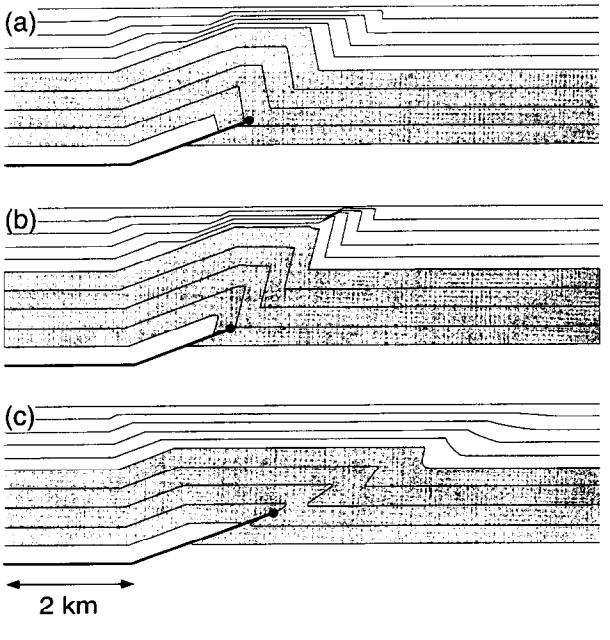


Fig. 22. Comparison of growth strata geometries associated with (a) fixed-axis kink band (b) constant-thickness kink band and (c) trishear fault-propagation folding models. For all models the ramp steps up at an angle of 20° from a flat detachment and the slip rate is constant at 1.0 m ka$^{-1}$ for a total run time of 1 Ma. Growth strata are recorded at intervals of 200 ka. The trishear apical angle is 5°. The fixed-axis fault-propagation and the trishear models propagate at twice the slip rate, while the constant thickness model propagates at 1.7 times the slip rate. Diffusion coefficient in all cases is 0.1 m$^2$ a$^{-1}$. Pre-growth strata are indicated by shading.

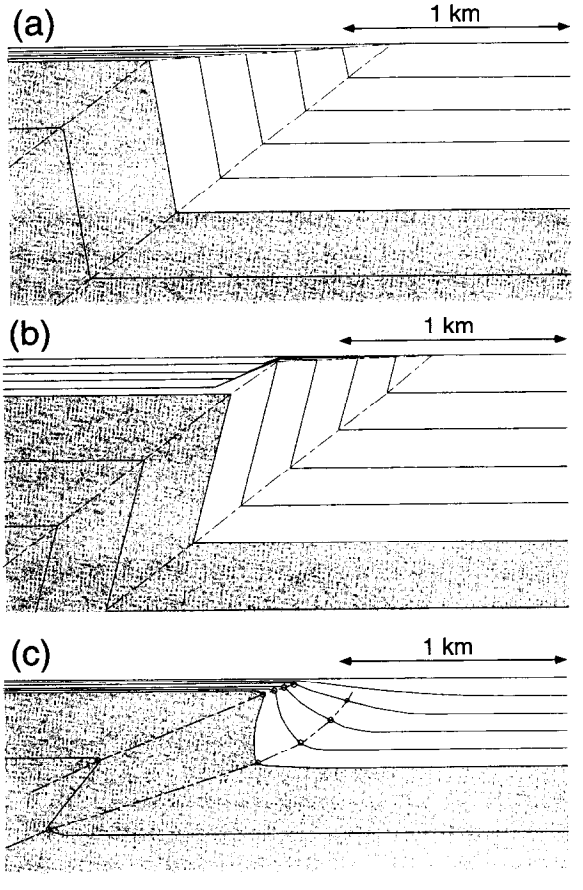


Fig. 23. Comparison of growth strata geometries associated with (a) fixed-axis kink band (b) constant-thickness kink band and (c) trishear fault-propagation folding. All model parameters are identical to Fig. 22 except that the base level rise has been reduced, and is 0.75 m ka$^{-1}$ in (a), 0.85 m ka$^{-1}$ in (b) and 0.4 m ka$^{-1}$ in (c). Axial surfaces are shown.

are shown. The rate of base level rise has, in all cases, been reduced in order to illustrate the growth geometries developed when sedimentation rate is only slightly higher than the maximum uplift rate of the structure. In the kink band models (Fig. 23a & b) the anticlinal axial surfaces are shallower (Fig. 22a). However, in the constant-thickness model (Fig. 23b) some of the complexities caused by material rolling from the overturned forelimb onto the crest of the structure can be observed. In the trishear model the synclinal axial surface shows a notable concave-up form which, in combination with the shallow dip of the anticlinal axial surface, results in weak upward convergence. This feature reminiscent of a growth triangle is commonly observed in trishear growth models. Although the two axial surfaces converge upwards they do not meet at a point at or below the depositional surface (as seen on profile 1, Fig. 7). Thus upward convergence of axial surfaces is not characteristic solely of kink band fault propagation folds and thus can have no implication for the process by which the fold developed.

In the third example (Fig. 24) the effect of a base level rise rate less than the uplift rate of the structures is illustrated. These conditions generate a fall-line (or a point in cross-section) separating erosional and depositional provinces. In the case of the kink band models the fall-line is located by the active synclinal axial surface, and the anticlinal axial surface in pregrowth strata passes upward into a foreland-dipping unconformity (Fig. 24a & b). In the trishear model the decrease causes an abrupt pinching out of growth strata at the fall-line, towards the crest of the structure (Fig. 24c).

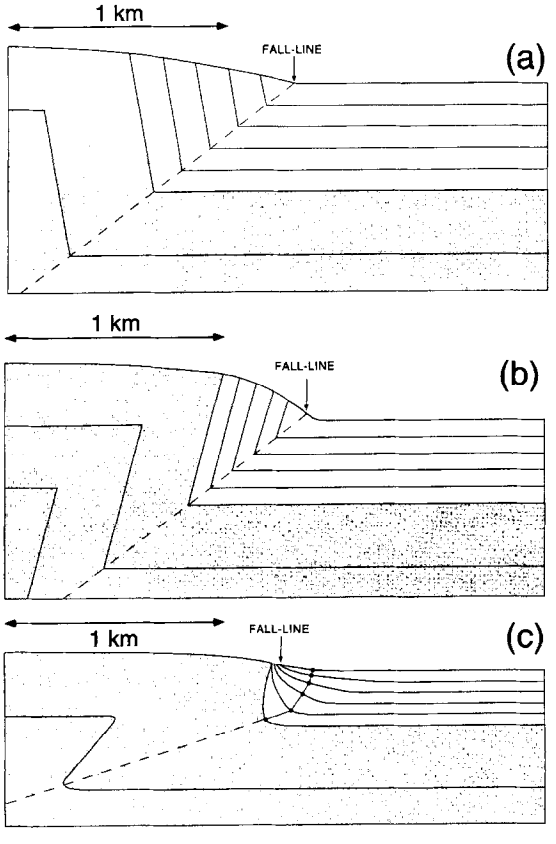


Fig. 24. Comparison of growth strata geometries associated with (a) fixed-axis kink band (b) constant-thickness kink band and (c) trishear fault-propagation folding. All model parameters are identical to Fig. 22 except that the base level rise is less than the uplift rate. Base level rise is 0.5 m $ka^{-1}$ in (a), 0.4 m $ka^{-1}$ in (b) and 0.25 m $ka^{-1}$ in (c). Diffusion coefficient in all cases is 0.1 $m^2$ $a^{-1}$. Axial surfaces are shown.

*Models for Sant Llorenç de Morunys profiles.* In this section the ability of the three models to account for the observed growth strata geometries in the three profiles of the Sant Llorenç de Morunys structure will be discussed. Regional data (Vergés, 1993) suggest that, if the geometries at Sant Llorenç de Morunys are to be linked to a fault at depth, then this fault may dip less than 20°. In comparison with the above model runs it is clear that, on the largest scale, during the growth of the structure, rates of sedimentation and uplift were approximately equivalent. This is demonstrated by growth strata thinning towards the structure and the shallowly-dipping anticlinal axial surfaces (Figs 7 & 9). The large-scale structure and detail of the growth strata for kink band and trishear models in an equivalent setting are shown in Fig. 25. All models can account for the sub-horizontal anticlinal axial surfaces seen in profiles 2 and 3 (Figs 9– 12). The synclinal axial surface in the trishear model is concave upwards (Fig. 25c) in agreement with that observed in all profiles, while those of the kink band models are planar. Curved hinges, as seen in the study area, are reproduced in the trishear model but not in the kink band migration models. The growth strata associated with the fixed-axis kink band model have a uniform steep dip throughout the forelimb but are nowhere overturned (Fig. 25a), while those associated with the constant-thickness model are overturned but show no variation in dip (Fig. 25b). The growth strata on the forelimb of the trishear model vary from overturned to horizontal (Fig. 25c). Both the fixed-axis and trishear models show thickness changes across the synclinal axial surface. In the fixed-axis kink band model the thickness changes are homogenous while in the trishear model they are emphasised in the synclinal region due to original stratigraphical thinning towards the anticline. While all models appear to account for the gross structure and stratigraphy moderately well, the trishear model accounts better for the internal stratigraphic geometries observed in profiles 2 and 3.

None of these models account for the large offset in the anticlinal axial surface observed in profile 1. This geometry suggests that there was an significant reduction and then increase in sedimentation rate in this area. Such an event is modelled in Fig. 26 where sedimentation stopped for a period of 400 ka and then resumed. The kink band models show a marked offset in the anticlinal axial surface which is complicated by the presence of locally derived packages of sediment (Fig. 26a & b). While the trishear model only produces a prominent

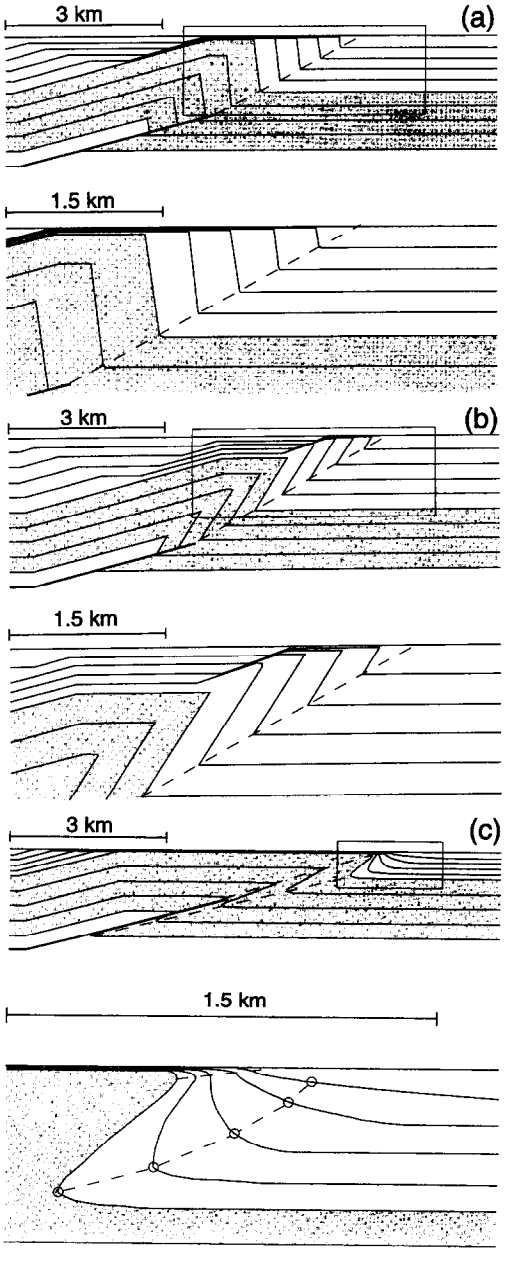


Fig. 25. Detail of growth strata geometries associated with (a) fixed-axis kink band (b) constant-thickness kink band and (c) trishear fault-propagation folding when background sedimentation rate (respectively 0.6 m $ka^{-1}$, 0.75 m $ka^{-1}$ and 0.27 m $ka^{-1}$) is approximately equal to uplift rate. Detail of growth strata geometries in the forelimb region (boxed area) is shown below each model. The ramp steps up at an angle of 15° from a flat detachment. For this step-up angle the constant thickness model has $p/s = 1.61$. The trishear apical angle is 5°. In the models the slip rate is constant at 1.0 m $ka^{-1}$ for a total run time of 2 Ma. Growth strata are recorded at intervals of 400 ka.

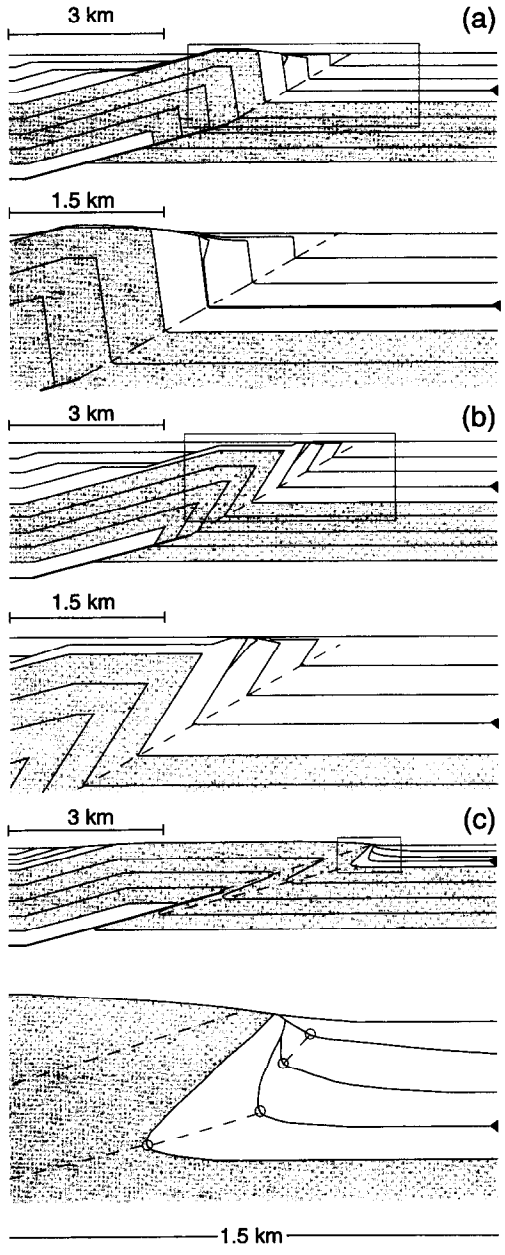


Fig. 26. Detail of growth strata geometries associated with (a) fixed-axis kink band (b) constant-thickness kink band and (c) trishear fault-propagation folding when there is a prolonged break in sedimentation. At 400 ka into the model run there was a break in sedimentation lasting 400 ka (marked by arrows). All other model parameters are as in Fig. 25. Detail of growth strata geometries in the forelimb region (boxed area) is shown below each model. The triangular units within growth strata in (a) and (b) are wedges of locally eroded material, deposited when there was no background sedimentation for 400 ka, and subsequently incorporated into the forelimbs.

onlap surface (Fig. 26c) with a simple pause in sedimentation, other more complex scenarios (such as variations in the rate of fault-propagation) can produce such jumps. Notably, in the trishear model the synclinal axial surface is displaced upward across the surface marking the sedimentation break. Such a feature is actually seen on profile 3 (Fig. 11). Kink band migration models cannot generate displacements of synclinal axial surfaces.

## DISCUSSION AND CONCLUSIONS

Structural field mapping indicates that: (1) at Sant Llorenç de Morunys a panel of overturned to sub-vertical growth strata passes southwards through a fold pair to essentially undeformed strata. (2) The asymmetrical fold pair comprises an anticline whose axial surface can be continuous or fragmented into en échelon segments and

which overall shows either a shallow hinterland, or sub-horizontal sheet-dip, and a syncline whose curved axial surface has a moderate hinterland dip. While converging upwards they do not meet at a point but become parallel or die out in the highest strata. (3) Principal and subsidiary angular unconformities are developed in the growth anticline and upper parts of the common limb. Composite offlap–onlap is observed in the growth syncline. (4) Major thickness changes occur across the anticlinal and synclinal axial surfaces and across the common limb. Dips shallow upward into younger beds within the common limb. (5) Significant along-strike variations in growth strata history partly correlate with an eastward increase in fold size. (6) An anticlockwise axially transecting cleavage exists in sandstones of the growth syncline hinge region. (7) Minor thrusts and strike-slip faults record brittle down-dip and along-strike extension in steep strata.

From these observations and sequential restoration of three NNE–SSW profiles, we conclude that the fold developed principally by progressive rotation of the common limb. Particle movement vectors for each horizon are arcuate about a hinterland pin-point. Deformation was ongoing at all levels of the fold so that, as the fold pair evolved, older strata became progressively more overturned and increasingly strained. At each stratigraphic level both hinges tightened through time as evidenced by cleavage strain in the syncline and shallowing of anticlinal axial plane segments in older strata. The gross evolution of the growth structure, detailed in geohistory periods 1 to 4, involved a gradual decrease in fold development while sedimentation continued. This process was diachronous, so that in the west (profile 1) post-growth strata overlapped and buried the structure while folding was still active in the east (profile 3).

There is a well-established correlation between fold wavelength and the thickness of the strata involved (Currie *et al.*, 1962). This implies that in an asymmetrical growth fold pair developing in a regime of continuous compression, where material is being continuously added, there should be no upper limit to fold wavelength apart from the ability of lithologies involved to accommodate the strain associated with steepening and overturning. The restored growth strata thus represent only the final stages (30%) of development of a large fold pair, which includes the entire steep panel of conglomerates and marine strata as illustrated in Fig. 3. We envisage the anticlinal hinge for these strata as a sub-horizontal zone of en échelon segments which lies above the present-day erosion surface, similar to the hinge zone documented in Figs 9 and 13. We suggest that the fold developed ahead of a propagating low angle blind thrust (Fig. 3). If the deformation were to have proceeded further, the foreland propagating thrust would have broken through the zone of highest strain in the common limb. The position of the fault tip is unknown but in a trishear model will depend on its $p/s$ ratio.

The Sant Llorenç de Morunys structure contains some general features predicted by both kink band and trishear numerical models (e.g. sub-horizontal anticlinal axial surfaces). However, only the trishear model can reproduce rounded hinges and the variation in bed dip and unit thickness seen in the common limb. Minor passive hinge migration is generated during limb rotation when combined with continuous addition of wedge shaped sedimentary bodies. The observed strain in the synclinal hinge is replicated only by the trishear model. Although axial surfaces converge upwards in the Sant Llorenç; fold pair, true growth triangles as generated by the kink band migration models are absent. The convergence of the axial surfaces and the concavity of the synclinal axial surface can be generated within the trishear model. Although the offset in the anticlinal axial surface in profile 1 may be easily reproduced by the kink band models, it can also be explained by more complex conditions in the trishear model. The observed displacement of the synclinal axial surface can only be generated within the trishear model. While a model involving principally non-rigid limb rotation (trishear) is at present most appropriate for the Sant Llorenç growth structure, it remains for a model to be developed which explains all of the features observed.

*Acknowledgements*—This work forms part of a multidisciplinary study into the evolution of growth folds in foreland basins, in collaboration with the European Union JOULE II Geosciences project *Integrated Basin Studies*. We wish to thank the Swiss *Bundesamt für Bildung und Wissenschaft* for funding (project number 94.0153). JV has been partially supported by DGICYT project PB94-0908 and by the Comissionat per Universitats i Recerca de la Generalitat de Catalunya, Quality Group GRQ94-1048. SH acknowledges the receipt of a Royal Society Postdoctoral Fellowship for which he is very grateful. We thank Martin Casey, Mark Cooper and Rob Butler for discussion regarding folding mechanisms and restoration techniques, Albert Martínez for information on Pyrenean geology and Francesc Sàbat for his hospitality in Barcelona. We also thank John Suppe for stimulating discussions in the field on kink band fold models. Himanshu Ghildyal and Pius Bissig are acknowledged for help with fieldwork, and T. R. Zapata, P. G. DeCelles and D. J. Anastasio for their reviews.

## REFERENCES

Allen, P. A. (1981) Sediments and processes on a small stream-flow dominated Devonian alluvial fan, Shetland Islands. *Sedimentary Geology* **29**, 31–66.

Allmendinger, R. W., Marrett, R. A. and Cladouhos, T. (1994) FaultKin version 3.8, Copyrighted Software.

Anadón, P., Cabrera, L., Colombo, F., Marzo, M. and Riba, O. (1986) Syntectonic intraformational unconformities in alluvial fan deposits, eastern Ebro basin margins NE Spain. In *Foreland Basins*, eds P. A. Allen and P. Homewood, pp. 259–271. Special Publication of the International Association of Sedimentologists **8**.

Blair, T. C. and McPherson, J. G. (1994) Alluvial fans and their natural distinction from rivers based on morphology, hydraulic processes, sedimentary processes, and facies assemblages. *Journal of Sedimentary Research* **A64**, 450–489.

Burbank, D. W. and Vergés, J. (1994) Reconstruction of topography and related depositional systems during active thrusting. *Journal of Geophysical Research* **99**, 20,281–20,297.

Burbank, D. W., Puigdefàbregas, C. and Muñoz, J. A. (1992) The chronology of the Eocene tectonic and stratigraphic development of the eastern Pyrenean foreland basin, northeast Spain. *Bulletin of the Geological Society, America* **104**, 1101–1120.

Currie, J. B., Patnode, H. W. and Trump, R. P. (1962) Development of folds in sedimentary strata. *Bulletin of the Geological Society, America* **73**, 655–674.

Dahlstrom, C. D. A. (1969) Balanced cross-sections. *Canadian Journal of Earth Sciences* **6**, 743–757.

DeCelles, P. G., Gray, M. B., Ridgway, K. D., Cole, R. B., Srivastava, P., Pequera, N. and Pivnik, D. A. (1991) Kinematic history of a foreland uplift from Palaeocene synorogenic conglomerate, Beartooth Range, Wyoming and Montana. *Bulletin of the Geological Society, America* **103**, 1458–1475.

DeCelles, P. G., Gray, M. B., Ridgway, K. D., Cole, R. B., Pivnik, D. A., Pequera, N. and Srivastava, P. (1991) Controls on synorogenic alluvial-fan architecture, Beartooth Conglomerate (Palaeocene), Wyoming and Montana. *Sedimentology* **38**, 567–590.

Elliott, D. (1976) The energy balance and deformation mechanisms of thrust sheets. *Philosophical Transactions of the Royal Society, London* **A283**, 289–312.

Epard, J.-L. and Groshong, R. H. (1995) Kinematic model of detachment folding including limb rotation, fixed hinges and layer-parallel strain. *Tectonophysics* **247**, 85–103.

Erslev, E. A. (1991) Trishear fault-propagation folding. *Geology* **19**, 617–620.

Erslev, E. A. and Rogers, J. L. (1993) Basement-cover geometry of Laramide fault-propagation folds. In *Laramide Basement Deformation in the Rocky Mountain Foreland of the Western United States*, eds C. L. Schmidt, R. B. Chase and E. A. Erslev, pp. 125–146. Special Publication of the Geological Society, America **280**.

Hails, J. R. (1976) Compaction and diagenesis of very coarse-grained sediments. In *Compaction of Coarse-grained Sediments, II*, eds G. V. Chilingarian and K. H. Wolf, *Developments in Sedimentology* Vol. 18B, pp. 445–473. Elsevier Scientific Publishing Company, Amsterdam.

Hardy, S. and Poblet, J. (1994) Geometric and numerical model of progressive limb rotation in detachment folds. *Geology* **22**, 371–374.

Hardy, S. and Poblet, J. (1995) The velocity description of deformation. Paper 2: sediment geometries associated with fault-bend and fault propagation folds. *Marine and Petroleum Geology* **12**, 165–176.

Hossack, J. R. (1979) The use of balanced cross-sections in the calculation of orogenic contraction. *Journal of the Geological Society, London* **136**, 705–711.

Jamison, W. R. (1987) Geometric analysis of fold development in overthrust terranes. *Journal of Structural Geology* **9**, 207–219.

Johnson, T. E. (1991) Nomenclature and geometric classification of cleavage-transected folds. *Journal of Structural Geology* **13**, 261–274.

Marshak, S. and Woodward, N. B. (1988) Introduction to cross-section balancing. In *Basic Methods of Structural Geology*, eds S. Marshak and G. Mitra, pp. 303–332. Prentice Hall, Englewood Cliffs, New Jersey.

Mató, E., Saula, E., Martínez, A., Muñoz, J. A., Vergés, J. and Escuer, J. (1994) Memoria explicative y cartografa geológica de la Hoja 293 (Berga) del mapa geológico de España Plan Magna a escala 1:50,000, I.T.G.E.

Mitra, S. (1990) Fault-propagation folds: geometry, kinematic evolution, and hydrocarbon traps. *Bulletin of the American Association of Petroleum Geologists* **74**, 921–945.

Mosar, J. and Suppe, J. (1992) Role of shear in fault-propagation folding. In *Thrust Tectonics*, ed. K. R. McClay, pp. 123–132. Chapman and Hall, London.

Nemec, W. and Steel, R. J. (1984) Alluvial and coastal conglomerates: their significant features and some comments on gravelly mass-flow deposits. In *Sedimentology of Gravels and Conglomerates*, eds E. H. Koster and R. J. Steel, pp. 1–31. Canadian Society of Petroleum Geologists Memoir **10**.

Nemec, W., Steel, R. J., Porebski, S. J. and Spinnangr, Å. (1984) Domba Conglomerate, Devonian, Norway: process and lateral variability in a mass flow-dominated, lacustrine fan-delta. In *Sedimentology of Gravels and Conglomerates*, eds E. H. Koster and R. J. Steel, pp. 295–320. Canadian Society of Petroleum Geologists Memoir **10**.

Nichols, G. J. (1987) Syntectonic alluvial fan sedimentation, southern Pyrenees. *Geological Magazine* **124**, 121–133.

Poblet, J. and Hardy, S. (1995) Reverse modelling of detachment folds; application to the Pico del Aguila anticline in the South Central Pyrenees (Spain). *Journal of Structural Geology* **17**, 1707–1724.

Puigdefàbregas, C., Muñoz, J. A. and Vergés, J. (1992) Thrusting and foreland basin evolution in the Southern Pyrenees. In *Thrust Tectonics*, ed. K. R. McClay, pp. 247–254. Chapman and Hall, London.

Puigdefàbregas, C. and Soquet, P. (1986) Tectono–sedimentary cycles and depositional sequences of the Mesozoic and Tertiary from the Pyrenees. *Tectonophysics* **129**, 173–203.

Ramsay, J. G. (1967) Folding and Fracturing of Rocks. International Series in the Earth and Planetary Sciences, McGraw-Hill Inc., New York.

Riba, O. (1967) Resultados de un estudio sobre el Terciario continental de la parte este de la depresión central catalana. *Acta Geológica Hispànica* **2**, 1–6.

Riba, O. (1973) Las discordancias sintectónicas del Alto Cardener (Prepirineo catalán), ensayo de interpretación evolutiva. *Acta Geológica Hispànica* **8**, 90–99.

Riba, O. (1976a) Tectonogenèse et Sedimentation: deux modèles de discordances syntectoniques pyrénéenes. *Bulletin of the Bureau de Recherche Géologie minerale 2ème séries, Sect I* **4**, 387–405.

Riba, O. (1976b) Syntectonic unconformities of the Alto Cardener, Spanish Pyrenees: a genetic interpretation. *Sedimentary Geology* **15**, 213–233.

Rich, J. L. (1934) Mechanics of low angle overthrust faulting as illustrated by the Cumberland thrust block, Virginia, Kentucky and Tennessee. *Bulletin of the American Association of Petroleum Geologists* **18**, 1584–1596.

Rust, B. R. and Koster, E. H. (1984) Coarse Alluvial Deposits. In *Facies Models*, ed. R. G. Walker, pp. 53–69. Geological Association of Canada, Toronto.

Schrader, F. (1988) Symmetry of pebble-deformation involving solution pits and slip-lineations in the northern Alpine Molasse basin. *Journal of Structural Geology* **10**, 41–52.

Soper, N. J. (1986) Geometry of transecting, anastomosing solution cleavage in transpression zones. *Journal of Structural Geology* **8**, 937–940.

Suppe, J. (1983) Geometry and kinematics of fault-bend folding. *American Journal of Science* **283**, 684–721.

Suppe, J. and Medwedeff, D. A. (1990) Geometry and kinematics of fault-propagation folding. *Eclogae Geologicae Helvetiae* **83**, 409–454.

Suppe, J., Chou, G. T. and Hook, S. C. (1992) Rates of folding and faulting determined from growth strata. In *Thrust Tectonics*, ed. K. R. McClay, pp. 105–121. Chapman and Hall, London.

Vergés, J. (1993) Estudi geològic del vessant sud del Pirineu oriental i central Evolució cinemàtica en 3D. Unpublished Ph.D thesis, Universitat de Barcelona.

Vergés, J., Burbank, D. W. and Meigs, A. (1996) Unfolding: an inverse approach to fold kinematics. *Geology* **24**, 175–178.

Waltham, D. and Hardy, S. (1995) The velocity description of deformation. Paper 1: theory. *Marine and Petroleum Geology* **12**, 153–163.

Williams, G. D. and Chapman, T. J. (1983) Strain developed in the hangingwall of thrusts due to their slip/propagation rate: a dislocation model. *Journal of Structural Geology* **5**, 563–571.